thickness) were cut by using an ultramicrotome. For immunolabeling, sections were incubated with primary antibody against P45017α (1:1,000) or P450arom (1:500) overnight and incubated with secondary gold-tagged (10 nm) Fab fragment in Tris-buffered saline. Sections were counterstained with 1% uranyl acetate and viewed on an electron microscope. For detailed description of the procedures, see *Supporting Text*.

Western Immunoblot Analysis. Microsomes were prepared as described in *Supporting Text* (8). After gel electrophoresis and the transfer to poly(vinylidene fluoride) membranes (Immobilon-P; Millipore), the blots were probed with antibodies against P45017α and P450arom at 1/5,000 dilution and incubated with biotinylated goat anti-rabbit IgG. The membranes were incubated with streptavidin–horseradish peroxidase complex. The protein bands were detected with ECL plus Western blotting detection reagents (Amersham Pharmacia).

RT-PCR and Southern Hybridization. The purified RNAs from rat tissues were reverse-transcribed by using a T-primed first-strand kit (Amersham Pharmacia) (22). Specific primer pairs and the PCR protocols are described in *Supporting Text*. For semiquantitative analysis (see ref. 23), the RT-PCR products were separated on 1.5% agarose gels, stained with ethidium bromide, and analyzed with a fluorescence gel scanner (Atto) and NIH IMAGE software, in comparison with standard curves obtained from PCR of diluted reverse transcribed products (between 1/100 and 1/10,000 in dilution), from testis, ovary, or liver. The PCR products were cloned into TA-cloning vector (Promega) and sequenced. The resulting sequence was identical to the reported cDNA sequences. These cloned products were used as DNA probes for Southern hybridization. After transfer of the RT-PCR products to nylon membrane, Southern hybridization was performed with ^{32}P-labeled cDNA probes for P45017α, P450arom, and GAPDH. Signals were measured by using a BAS-1000 Image analyzer (Fuji film).

HPLC Analysis. Procedures were essentially the same as described in ref. 8. Briefly, the hippocampal cubic slices were incubated with 5×10^6 cpm of [^{3}H]steroids at 28°C in a 1.2 mM Mg^{2+} physiological saline (pH 7.2, consisting of 5 mM Hepes, etc.), into which 95% O_2 gas was bubbled. [^{3}H]steroids (DHEA, estradiol, etc.) were purchased from New England Nuclear, and their specific activities were 22.5–105 Ci/mmol (1 Ci = 37 GBq). After termination of the reaction, the slices were homogenized. To extract steroid metabolites, ethyl acetate/hexane (3:2) was applied to the homogenates. The organic phase was collected by centrifugation, dried, dissolved in an elution solvent of HPLC, and filtrated. The metabolites were separated by using an HPLC system (Jasco, Tokyo). For detailed description of the procedures, see *Supporting Text*.

RIA Analysis. Procedures were essentially the same as described in ref. 8. Briefly, plasma was prepared from trunk blood collected from decapitated rats. The hippocampal cubic slices were incubated at 37°C in 0.1 mM Mg^{2+} physiological saline into which O_2 gas was bubbled. Extraction of steroids were performed as described in HPLC analysis. The estradiol or DHEA fractions were separated by using HPLC with solvent A, and reconstituted in a 0.1 M sodium phosphate buffer containing 0.1% gelatin. The concentration of steroids was measured by means of RIA, which was a competitive reaction assay, for example, between purified estradiol and exogenously added [^{3}H]estradiol against estradiol IgG. Anti-steroid IgG was from ICN. For a detailed description of the procedures, see *Supporting Text*.

Results

Localization and Presence of Cytochrome P450s. Light microscopic investigations of the immunohistochemical staining were performed to determine the cell-specific localization of P45017α and P450arom in the hippocampal formation of adult male rats. Intense

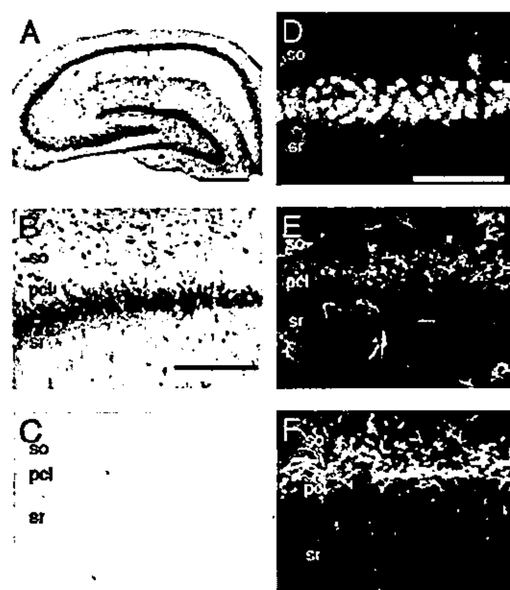

Fig. 1. Immunohistochemical staining of P45017α in the hippocampal formation of an adult male rat. (*A*) The coronal section of the whole hippocampal formation. (*B*) The CA1 region. (*C*) The CA1 stained with anti-P45017α IgG preadsorbed with purified P45017α. (*D*) Fluorescence dual staining of P45017α (green) and neuronal nuclear antigen (red). (*E*) Fluorescence dual staining of P45017α (green) and glial fibrillary acidic protein (red). (*F*) Fluorescence dual staining of P45017α (green) and myelin basic protein (red). In *D–F*, superimposed regions of green and red fluorescence are represented by yellow. so, stratum oriens; pcl, pyramidal cell layer; sr, stratum radiatum. (Scale bar, 800 μm for *A* and 120 μm for *B–F*.)

immunoreactions with anti-P45017α IgG (Fig. 1) and anti-P450arom IgG (Fig. 2) were restricted to pyramidal neurons in the CA1–CA3 regions and to granule cells in the dentate gyrus. The staining shows P45017α and P450arom to be distributed over the entire cell body, in general, and also along the dendrites of the pyramidal neurons in the CA3 region. Neurons were stained with IgG against neuronal nuclear antigen (NeuN). The colocalization of neurons with P45017α and P450arom was demonstrated by using fluorescence dual labeling procedures. Although the NeuN and P450 stainings were nearly superimposed, this was due to the

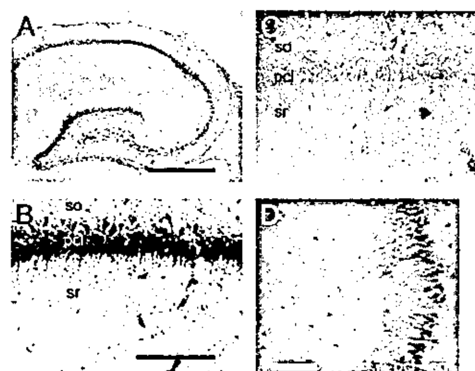

Fig. 2. Immunohistochemical staining of P450arom in the hippocampal formation of an adult male rat. (*A*) The coronal section of the whole hippocampal formation. (*B*) The CA1 region. (*C*) The CA1 stained with P450arom IgG preadsorbed with purified P450arom. (*D*) The CA3, where not only cell bodies but also processes of neurons are densely stained. so, stratum oriens; pcl, pyramidal cell layer; sr, stratum radiatum. (Scale bar, 800 μm for *A* and 120 μm for *B–D*.)

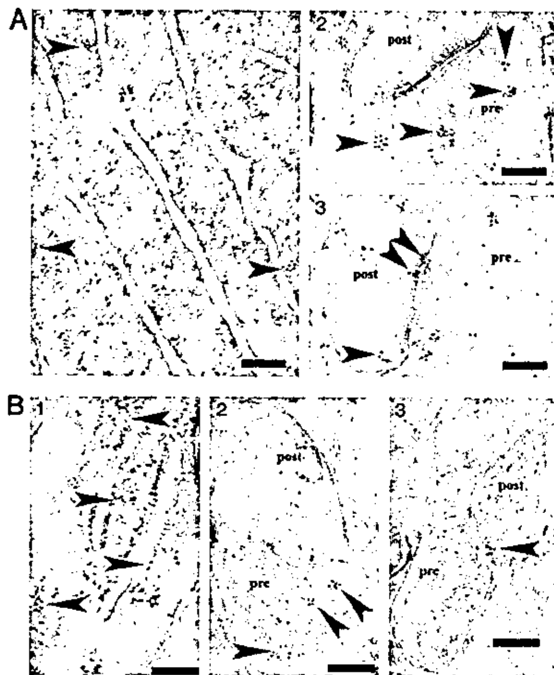

Fig. 3. Immunoelectron microscopic analysis of the distribution of P45017α (*A1–A3*) and P450arom (*B1–B3*) within axospinous synapses, in the strata radiatum of the hippocampal CA1 region at the central region of the rostrocaudal level. Gold particles (indicated with arrowheads) were observed to be localized in the endoplasmic reticulum (*A1* and *B1*), the presynaptic region (*A2* and *B2*), and the postsynaptic region (*A3* and *B3*) of pyramidal neurons. In the axon terminal (*A2* and *B2*), gold particles were associated with small synaptic vesicles (*A2* and *B2*). In dendritic spines, gold particles were found within the head of the spine (*A3* and *B3*). Pre, presynaptic region; Post, postsynaptic region. (Scale bar, 200 nm.)

localization of these cytochromes in the endoplasmic reticulum. distributed over the entire cell bodies, and thus did not indicate a nuclear localization of the cytochromes. Preadsorption of the antibody with an excess of purified guinea pig P45017α or human P450arom antigen (30 μg/ml) resulted in a complete disappearance of the immunoreactivity of these P450s, in all of the positively stained cells in the hippocampus.

The distribution of glial cells was investigated by the immunostaining of marker proteins. Antibodies against glial fibrillary acidic protein (GFAP) of astrocytes, stained star-shaped cells in the strata radiatum, and oriens in the hippocampus. IgG against myelin basic protein (MBP) of oligodendrocytes stained many long fibril cells in the hippocampus. Most of the cells stained with GFAP and MBP IgG were lacking in immunoreactivity to IgG against P45017α and P450arom. This indicates that most of the P45017α- and P450arom-containing cells are neither astrocytes nor oligodendrocytes.

The neuronal localization of P450 was further clarified by ultrastructural investigations. An immunoelectron microscopic analysis using postembedding immunogold was performed to determine the subcellular localization of P45017α and P450arom in hippocampal neurons of adult male rats. P45017α (Fig. 3*A*) and P450arom (Fig. 3*B*) were localized not only in the endoplasmic reticulum but also in both the axon terminals and dendritic spines of principal neurons. Gold particles were clustered in the endoplasmic reticulum of neurons. Gold particles were also localized within the presynaptic compartments, as well as within the postsynaptic compartments. In the presynaptic terminals, gold particles were primarily associated with synaptic vesicles. In dendrites, gold particles were distributed within the cytoplasm of the head of the spine. In some cases, gold particles were affiliated within the postsynaptic density. Preadsorp-

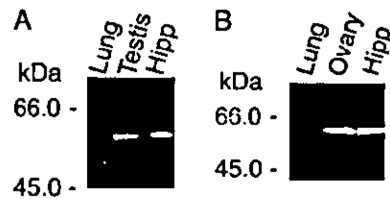

Fig. 4. Western immunoblot analysis of P45017α (*A*) and P450arom (*B*) in microsomes from adult rat. (*A*) Lung (50 μg protein), testis (1 μg), and hippocampus (50 μg). (*B*) Lung (50 μg protein), ovary (1 μg), and hippocampus (50 μg). Lung was used as a negative control.

tion of the antibody with an excess of P45017α or P450arom antigen (30 μg/ml) resulted in a complete disappearance of the immunoreactivity of these P450s, in all of the positively stained cells.

There were essentially no significant differences between P45017α and P450arom concerning their topographical distribution in neurons. Investigations were performed mainly in the stratum radiatum of the CA1; however, the intraneuronal distribution of gold particles was essentially identical in the CA1, CA3, and dentate gyrus.

The presence of P45017α and P450arom proteins was verified by Western immunoblot analysis. In hippocampal microsomes, single protein bands were observed for P45017α and P450arom (Fig. 4). The concentration of P45017α and P450arom was ≈1/100th to 1/200th of that typical of the testis (P45017α) and ovary (P450arom). The electrophoretic mobility of the P45017α and P450arom bands indicated a molecular mass of ≈57 kDa and 58 kDa, respectively. These molecular masses were approximately equal to those in testis and ovary. Protein bands disappeared when either antibodies were preadsorbed with purified P450 antigens (30 μg/ml).

The level of mRNA transcripts for P45017α and P450arom was investigated by using RT-PCR analyses. The relative number of P450 transcripts expressed in the hippocampus (Fig. 5, lane 5) from adult male rats was demonstrated to be ≈1/200th to 1/300th of those expressed in the testis and ovary, for P45017α and P450arom, respectively. The mRNA levels for P45017α and P450arom in the hypothalamus (Fig. 5, lane 6) were slightly greater (by ≈1.5-fold) than those obtained in the hippocampus. On the other hand, the level of P45017α mRNA in the cerebral cortex (Fig. 5, lane 4) and cerebellum (Fig. 5, lane 7), was $<10^{-4}$ and 10^{-3}, respectively relative to levels observed in the testis. The level of P450arom mRNA, relative to levels in the ovary, was ≈1/500 in the cerebral cortex (Fig. 5, lane 4) and cerebellum (Fig. 5, lane 7).

The expression level of mRNA transcripts for 17β-hydroxy-

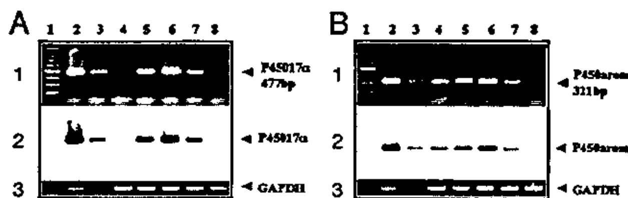

Fig. 5. RT-PCR analysis of mRNAs for P45017α (*A*) and P450arom (*B*) in the adult rat. The RT-PCR products (50 ng each) were visualized with ethidium bromide in *Top*. (*A*) Lane 1, marker (100-bp ladder); lane 2, testis diluted at 1 100; lane 3, testis diluted at 1/1,000; lane 4, cerebral cortex; lane 5, hippocampus; lane 6, hypothalamus; lane 7, cerebellum; lane 8, peripheral blood leukocytes. (*B*) Lane 1, marker; lane 2, ovary diluted at 1/100; lane 3, ovary diluted at 1 1,000; lane 4, cerebral cortex; lane 5, hippocampus; lane 6, hypothalamus; lane 7, cerebellum; lane 8, liver. Peripheral blood leukocytes and liver were used as the negative controls. (*Middle*) Southern hybridizations. (*Bottom*) Ethidium bromide staining of GAPDH.

PHARMACOLOGY

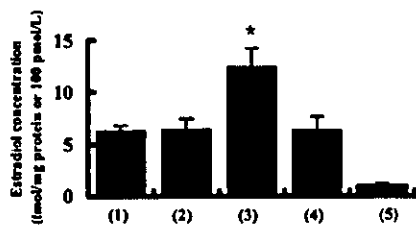

Fig. 6. RIA analysis of estradiol concentrations in adult male rats. Estradiol concentration in the hippocampus before incubation (basal) (column 1), the hippocampus after a 30-min incubation without NMDA (column 2), the hippocampus after a 30-min incubation with 100 μM NMDA (column 3), the hippocampus after a 30-min incubation with 100 μM NMDA in the presence of MK-801 (column 4), and plasma (column 5). The vertical axis indicates the estradiol concentration in fmol/mg protein for the hippocampus (columns 1–4) and in fmol/μl for plasma (column 5). The significance of the NMDA-induced production of estradiol was confirmed by using the Student *t* test (*, $P < 0.05$). The data represent an average over three independent experiments.

steroid dehydrogenase (17β-HSD) (types 1–4) was also investigated by using RT-PCR (data not shown). The level of 17β-HSD mRNA observed in the hippocampus was ≈1/10th relative to the level in the ovary for 17β-HSD (type 1), 1/200th to 1/300th relative to the level in the testis for 17β-HSD (type 3), roughly the same relative to the level in the liver for 17β-HSD (type 4), and $<10^{-3}$ for 17β-HSD (type 2) relative to the level in the liver.

Steroid Metabolism Assay. The synthesis of estradiol in hippocampal slices was examined by means of a specific RIA using estradiol antibody (ICN) (Fig. 6). The basal concentration of estradiol observed in the hippocampus was 0.60 ± 0.05 fmol/mg wet weight (6.3 ± 0.5 fmol/mg protein; mean ± SEM from three independent experiments). The estradiol basal concentration in the plasma was 0.098 ± 0.039 fmol/μl (≈1.02 fmol/mg protein or 0.098 fmol/mg wet weight), a value considerably lower than that observed in the hippocampus. The *N*-methyl-D-aspartate (NMDA)-inducible production of estradiol was measured by stimulating hippocampal slices with 100 μM NMDA (Biomol) for 30 min. at 37°C in a 0.1 mM Mg^{2+} medium. This treatment increased the concentration of estradiol to 1.35 ± 0.18 fmol/mg wet weight (13.0 ± 1.7 fmol/mg protein), which is nearly twice the estradiol level in hippocampal slices incubated for 30 min without NMDA. Stimulation of net estradiol production with NMDA was completely suppressed by the application of 50 μM MK-801 (a specific blocker of NMDA receptors, Sigma). This enhancement in estradiol synthesis may be due to an increase in the NMDA receptor-mediated Ca^{2+} influx that drives the transport of cholesterol to the inner membrane of mitochondria, followed by a cascade of steroidogenesis (7). The basal concentration of DHEA was also measured in the hippocampus and plasma. The concentration of DHEA was 0.28 ± 0.07 fmol/mg wet weight (2.7 ± 0.7 fmol/mg protein) in the hippocampus, and 0.075 ± 0.036 fmol/μl in plasma. These values are in reasonable agreement with previous publications using DHEA extracts from the whole brain (6).

To analyze the pathway of steroidogenesis, the metabolism of radioactive steroids in hippocampal slices was investigated by using HPLC. To observe the conversion of PREG to DHEA, hippocampal cubic slices from adult male rats were incubated for 0, 1, 3, and 5 h at 28°C, using 5 × 10^6 cpm of [7-^{3}H]PREG as a precursor. Careful attention was given to the removal of all fats from the hippocampal slices during the purification of steroids, before the application to HPLC. A portion of the purified radioactive metabolites (total of 10^6 cpm) was analyzed with an HPLC system, which used an elution liquid composed of hexane/isopropanol/acetic acid (97:3:1) (solvent A). The principal radioactive peak in the tritiated metabolite exhibited a retention time of ≈9.5 min, which was the same as that of [^{14}C]DHEA used as a standard (Fig. 7A). A time-dependent increase in the [^{3}H]DHEA fractions was observed over a period of 5 h (Fig. 8A, which is published as supporting

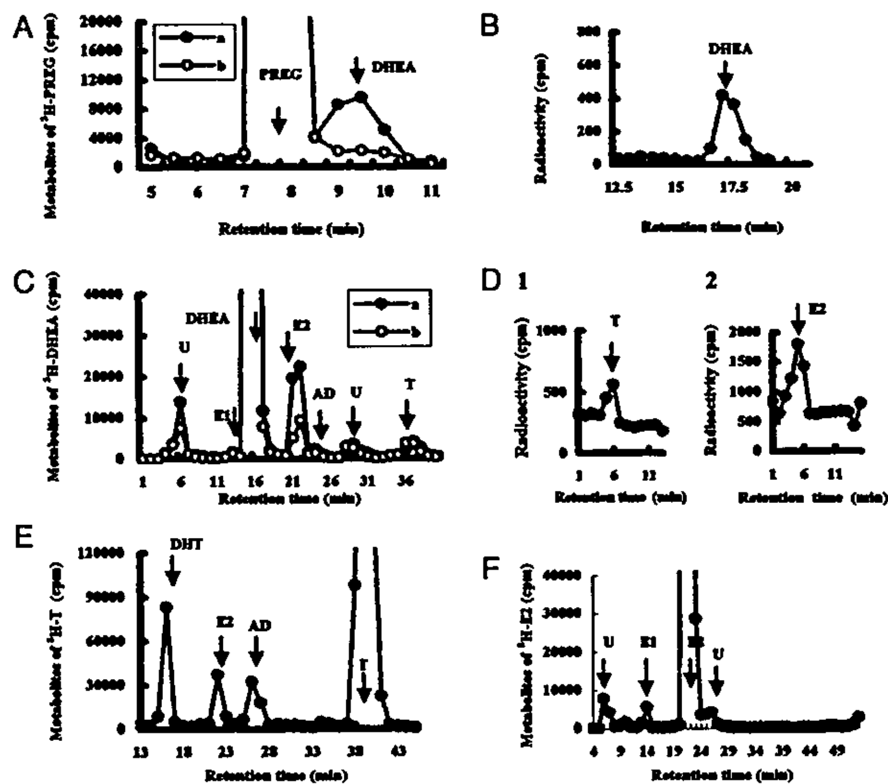

Fig. 7. HPLC analysis of steroid metabolism in adult rat hippocampal slices. A total of 10^6 cpm purified metabolites were applied to HPLC. (*A*) HPLC profiles of [^{3}H]PREG metabolites using elution solvent A. Slices were incubated for 5 h in the absence (line a) or in the presence (line b) of SU-10603. (*B*) Reverse-phase HPLC (solvent C) of [^{3}H]DHEA fractions from line a in *A*. (*C*) Profiles of [^{3}H]DHEA metabolites (solvent B) in the absence (line a) or in the presence (line b) of fadrozole, after incubation of slices for 5 h. (*D*) Reverse-phase HPLC (solvent C) of [^{3}H]testosterone (*D1*) and [^{3}H]estradiol (*D2*) taken from peaks T and E2, respectively, in *C*. (*E*) Profiles (solvent B) of [^{3}H]testosterone metabolites after incubation of slices for 5 h. (*F*) Profiles (solvent B) of [^{3}H]estradiol metabolites after a 5-h incubation. The arrows designate the elution peak position of the standard [^{14}C]steroid with abbreviations: E1 (estrone), T (testosterone), and E2 (estradiol). "U" designates unknown metabolites. The vertical axis indicates ^{3}H radioactivity (cpm). The retention time of the (same) standard [^{14}C]steroid differed slightly among *C*, *E*, and *F* due to the different silica gel columns used. More than three independent experiments were performed for each of these analyses.

PNAS PNAS PNAS

information on the PNAS web site). Analysis of the steroid extract (adjusted to a total of 10^6 cpm) indicated that the amount of [^{3}H]DHEA (product), relative to [^{3}H]PREG (substrate), increased from $0.0 \times 10^4/1.0 \times 10^6$ (0 h) to $1.0 \times 10^4/0.98 \times 10^6$ (1 h), $2.9 \times 10^4/0.97 \times 10^6$ (3 h), and $4.6 \times 10^4/0.96 \times 10^6$ (5 h). Note that trilostane (Mochida) was included in these experiments to facilitate observation of the net production of [^{3}H]DHEA by inhibiting 3β-hydroxysteroid dehydrogenase (3β-HSD). Trilostane prevents the conversion of DHEA to AD and of PREG to progesterone. The application of a specific inhibitor of P45017α, SU-10603 (Novartis) at 10 μM, reduced the production of [^{3}H]DHEA to ≈21% of the control value. To exclude the possibility of contamination from other radioactive metabolites, the three fractions having a retention time of 9–10 min were combined and subjected to a second round of HPLC analysis. The column was eluted with a different elution solvent B (hexane/isopropanol/acetic acid = 98:2:1) for the normal phase HPLC (Fig. 8*B*), and with solvent C (acetonitrile/H_2O = 40:60) for the reverse-phase HPLC (Fig. 7*B*), to improve the resolution. A single radioactive peak of [^{3}H]metabolite having the same retention time as that of [^{14}C]DHEA was observed in this second round of HPLC. These results indicate the significant enzymatic activity of P45017α in the hippocampus, which is responsible for the conversion of PREG to DHEA.

To investigate the conversion of DHEA to testosterone and estradiol, hippocampal slices were incubated with 5×10^6 cpm of [1,2,6,7-^{3}H]DHEA for 5 h at 28°C, and the purified metabolites (total of 10^6 cpm) were analyzed by using HPLC. When elution solvent B was used, several eluent peaks were observed (Fig. 7*C*). The eluent peak with a retention time of 37 min was designated as testosterone by comparison with the standard [^{14}C]testosterone. The eluent peak exhibiting a retention time of 21–22 min was close to the position of [^{14}C]estradiol. To improve the resolution, these fractions were collected and subjected to a second round of HPLC analysis using solvent D (hexane/isopropanol/acetic acid = 99:1:1). A single peak, with a retention time of 51 min, was observed, which is in good agreement with [^{14}C]estradiol (Fig. 8*C*). An additional round of analysis, using reverse-phase HPLC and solvent C, was performed for the HPLC fractions corresponding to estradiol, testosterone, and AD. These metabolites were again observed to elute at the same positions obtained for the standard [^{14}C]steroids (Fig. 7*D*). Analysis of the steroid extract (10^6 cpm) indicated that the relative amount of [^{3}H]estradiol (product) to [^{3}H]DHEA (substrate) increased from $0.0 \times 10^4/1.0 \times 10^6$ (0 h) to $3.5 \times 10^4/0.90 \times 10^6$ (1 h), $5.5 \times 10^4/0.88 \times 10^6$ (3 h) and $6.4 \times 10^4/0.86 \times 10^6$ (5 h).

To confirm the participation of P450arom in estradiol synthesis, fadrozole (Novartis) was used to inhibit the activity of P450arom. A 30-min preincubation with 100 μM fadrozole, applied before the addition of [^{3}H]DHEA, suppressed the conversion of [^{3}H]DHEA to estradiol considerably (to ≈34% of the control), but had no suppressive effect on its conversion to testosterone (to ≈102% of the control) (Fig. 7*C*). The conversion from testosterone to estradiol and dihydrotestosterone (DHT) was then investigated. Hippocampal slices were incubated with [1,2,6,7-^{3}H]testosterone (5×10^6 cpm) for 0, 1, 2, 3, 4, and 5 h at 28°C, and the purified metabolites (total of 10^6 cpm) were analyzed with HPLC using solvent B (Fig. 7*E*). A time-dependent increase in [^{3}H]estradiol, [^{3}H]DHT, and [^{3}H]AD was observed (Fig. 8*D*). Analysis of the steroid extracts (10^6 cpm) indicted that the relative amount of [^{3}H]estradiol (product) to [^{3}H]testosterone (substrate) increased from $0.0 \times 10^4/1.0 \times 10^6$ (0 h) to $0.7 \times 10^4/0.90 \times 10^6$ (1 h), $1.9 \times 10^4/0.87 \times 10^6$ (3 h) and $3.8 \times 10^4/0.84 \times 10^6$ (5 h). The absence of other contaminating metabolites in these estradiol fractions was confirmed by means of a second round of HPLC using solvent C (for normal phase HPLC) and D (for reverse-phase HPLC).

HPLC analysis of AD and estrone metabolites are described in *Supporting Text*. Finally, the conversion of estradiol to other metabolites was also investigated by incubating [2,4,6,7-^{3}H]estradiol (5×10^6 cpm) with hippocampal slices for 5 h. Only very small amounts of metabolites such as estrone and testosterone were observed (Fig. 7*F*), suggesting that estradiol was not significantly inactivated but may remain stable.

Discussion

Our results not only demonstrated the distribution of P45017α and P450arom in pyramidal and granule neurons at the light microscopic level (Figs. 1 and 2), but also indicated that these P450 proteins were specifically localized in pre- and post-synaptic locations and the endoplasmic reticulum of these neurons by electron microscopy, with a single molecule (gold particle) resolution (Fig. 3). These findings, combined with the results of steroid metabolism assays, strongly suggest that estradiol is endogenously synthesized in neurons from cholesterol in the hippocampal formation. These results indicate the need to reconsider the belief that these sex steroids are produced only in the gonads and reach the target brain via blood circulation. Rather, such steroids may be produced endogenously in the adult brain, where they play an essential role in the plasticity and protection of neurons.

Pathway of Steroidogenesis in the Hippocampus. In our previous work, the steroid synthesis was triggered by exposing neurons to NMDA, which induced a Ca^{2+} influx through the NMDA receptors and resulted in the significant production of PREG(s) (5, 7). A pool of full-length (37-kDa) steroidogenic acute regulatory protein (StAR) was processed to the truncated 30-kDa StAR upon NMDA stimulation (7). The expression of essential steroidogenic proteins [StAR, P450scc (CYP11A1), and 3β-HSD] in the hippocampal principal neurons was demonstrated by means of immunostaining and Western blot analysis (7–9) or by *in situ* hybridization (17, 22). The presence of mRNAs for 17β-HSD types 1–4 has been demonstrated in the human hippocampus (24). In the rat hippocampus, 17β-HSD (type 1) has been shown to be localized in neurons by immunostaining (25). Previous studies have shown the immunoreactivity of 5α-reductase in the rat hippocampus (16, 26).

In combination with these results, the current observations suggest that hippocampal neurons are equipped with a set of enzymes to catalyze the synthesis of estradiol from cholesterol. Neurosteroid synthesis may therefore proceed in the following manner. First, cholesterol is transported with StAR into the inner membrane of mitochondria, and converted to PREG by P450scc. After reaching the microsomes, P45017α converts PREG to DHEA. Then DHEA to AD by 3β-HSD, 17β-HSD (type 3) catalyzes the conversion of AD to testosterone. This is followed by a further transformation to estradiol by P450arom. It appears that estradiol is also formed by 17β-HSD (type 1) from estrone, which is converted from AD by P450arom.

The rate of production of steroid metabolites was rather low. The amount of [^{3}H]DHEA formed from [^{3}H]PREG, that of [^{3}H]estradiol from [^{3}H]DHEA, and that of [^{3}H]estradiol from [^{3}H]testosterone each represented ≈4.6–6.4% of the total radioactivity obtained by using [^{3}H]steroid precursors, observed after 5-h incubation (Fig. 7). Several reasons are considered for this. First, the binding of exogenously applied [^{3}H]steroid to P450s in hippocampal slices is likely to be very inefficient, as such steroids must penetrate deeply into cells in the thick slices to reach enzymes, without being absorbed by nonspecific binding to hydrophobic membranes, and replace endogenous steroid substrates already bound to the enzymes. Second, the conversion rate from [^{3}H]PREG to [^{3}H]DHEA by P45017α may indeed be extremely low; as a result, no previous study could detect this low activity. Third, not only [^{3}H]DHEA but also other steroids such as sulfated DHEA and 7-hydroxyDHEA (27) may be produced in parallel from [^{3}H]PREG. Fourth, [^{3}H]estradiol is not a unique metabolite from [^{3}H]testosterone, but DHT and other steroids may also be produced in parallel. These multiple pathways, including backward reactions, may be a primary reason of the observed low efficiency of steroid metabolism, because of the

PHARMACOLOGY

presence of sulfotransferase, 5α-reductase, and cytochrome P4507b (16, 26, 28). These factors could reduce the rate of production for [^{3}H]DHEA and [^{3}H]estradiol to 4.6–6.4% of the total radioactivity.

To verify that the observed low levels of radioactive metabolites were real products, we performed a set of control experiments. We observed a considerable decrease in [^{3}H]DHEA production by the presence of SU-10603, inhibitor of P45017α (Fig. 7A). In addition, estradiol production was suppressed considerably by the presence of fadrozole, an inhibitor of P450arom (Fig. 7C). These results indicate that the observed steroid metabolite levels are above the detection limit of the HPLC analysis. The background radioactivity in the HPLC profiles in Fig. 7 was <300 cpm at any position, using hippocampal slices fixed with paraformaldehyde to inactivate steroidogenic enzymes before incubation with ^{3}H-substrate steroids.

Glial cells have been considered to play an important role in neurosteroidogenesis, as many reports have indicated the presence of mRNA and steroidogenic activity for P450scc, P45017α, 3β-HSD, and 17β-HSD in cultures of astrocytes and oligodendrocytes (6, 11, 12, 29, 30). Based on these studies, the following steroidogenic sequence is suggested in the neonatal rat brain. The primary source of PREG is the oligodendrocytes. PREG is then transferred to the astrocytes, where it is converted to DHEA, and further metabolized to sex steroids (11, 12). It should be noted, however, that these studies, which use primary glial cell cultures, can be performed only for embryonic and neonatal brain. As a result, direct information is not available from these studies regarding the biosynthesis of neurosteroids in adult rat brain. The possibility of glial steroidogenesis in the adult hippocampal formation cannot be excluded by the present study, as a weak staining of P450scc (7), P45017α, and P450arom was observed in some glia-like cells.

Previous Understanding of P45017α and P450arom in the Brain. A direct demonstration of the neuronal synthesis of DHEA in adult mammalian brain has not previously been reported, although the presence of significant amounts of DHEA had been noted (15, 10). It has therefore been assumed that DHEA and the sex steroids are supplied to the brain via the blood circulation (6, 15, 20). As reported in a number of studies, the absence of P45017α and its activity in the brain of adult mammals has discouraged the investigation of the endogenous synthesis of sex steroids and DHEA in adult brain (13–16). Incubations of [^{3}H]PREG with brain slices and microsomes from rat and mouse, had failed to produce [^{3}H]DHEA (15). Moreover, many attempts to demonstrate the immunohistochemical reactivity for P45017α in the rat brain had been unsuccessful (13). mRNAs for P45017α had not been detected in adult rat brain by either RNase protection assays or RT-PCR (14). The expression of the mRNA for P45017α had been reported by many laboratories as only transient, occurring during rat embryonic and neonatal development (11, 12, 31). Although a similar level of P45017α mRNA had been reported in both astrocytes and neurons in primary cultures from the brain of neonatal rats, neurons had exhibited a much lower metabolic activity than astrocytes for the conversion of PREG to DHEA (11, 12). Such investigations, which use primary cell cultures, are not possible for adult brains, because cells from adult brains cannot be cell cultured.

Our observation of a significant amount of P45017α mRNA was achieved due to (*i*) a careful design of primers to not include sequences that may form stable loops, inhibiting binding to mRNA, (*ii*) the use of isolated rat hippocampal formation, rather than brain mixtures where the cortex did not express P45017α mRNA, and (*iii*) the considerable improvement in the last few years of the commercially available enzymes such as *Taq* polymerase used for RT-PCR.

The role of P450arom in the hippocampus had also not been well elucidated, primarily because many studies had indicated the absence of P450arom in the adult rat and mouse hippocampus (20, 32). Recently, however, the significant expression of mRNA for P450arom in the pyramidal and granule neurons of the adult rat hippocampus has been demonstrated by using *in situ* hybridization (17). The level of the mRNA expression in the adult mouse hippocampus was approximately half of that in neonatal stages (23). The activity of P450arom has been suggested in the adult male rat hippocampus based on the results of the testosterone-induced protection of the hippocampal neuronal death induced by the domoic acid-treatments (3).

Modulation by Estradiol of Hippocampal Neurons. Investigations have been focused on female rats regarding the chronic, delayed effects of estradiol on synaptic plasticity. For example, the dendritic spine density in pyramidal neurons is sensitive to the estrous cycle (1, 33) and also to experimentally induced estrogen depletion and replacement, which serve to modulate estrogen levels in blood circulation (4). Estradiol also induces rapid effects. A 20-min preperfusion of 1–10 nM estradiol induced the rapid modulation of long-term potentiation of the CA1 neurons in the hippocampal slices (2). Our elucidation of the estradiol-synthesis in principal neurons, which begins with cholesterol, introduces an essentially a new supply of brain neurosteroids, in addition to gonads. Estradiol synthesis may be dependent on NMDA receptor-mediated Ca^{2+} influx, thereby dependent on synaptic communication (5, 7). The concentration of endogenously synthesized estradiol by NMDA stimulation (≈0.75 nM; see Fig. 6, column 3) should be sufficient to modulate these neuronal activities, because the local concentration of estradiol (at the site of synthesis) may transiently be an order of magnitude higher than the mean concentration of 0.75 nM.

We thank Dr. J. Rose for critical reading of the manuscript. We thank Novartis for the kind gift of SU-10603. This work was supported in part by National Institutes of Health Grant PO1AG16765 (to J.H.M.)

1. Woolley, C. S., Weiland, N. G., McEwen, B. S. & Schwartzkroin, P. A. (1997) *J. Neurosci.* **17**, 1848–1859.
2. Foy, M. R., Xu, J., Xie, X., Brinton, R. D., Thompson, R. F. & Berger, T. W. (1999) *J. Neurophysiol.* **81**, 925–929.
3. Azcoitia, I., Sierra, A., Veiga, S., Honda, S., Harada, N. & Garcia-Segura, L. M. (2001) *J. Neurobiol.* **47**, 318–329.
4. Pozzo-Miller, L. D., Inoue, T. & Murphy, D. D. (1999) *J. Neurophysiol.* **81**, 1404–1411.
5. Shibuya, K., Takata, N., Hojo, Y., Furukawa, A., Yasumatsu, N., Kimoto, T., Enami, T., Suzuki, K., Tanabe, N., Ishii, H., *et al.* (2002) *Biochim. Biophys. Acta* **25462**, 1–16.
6. Baulieu, E. E. (1997) *Recent Prog. Horm. Res.* **52**, 1–32.
7. Kimoto, T., Tsurugizawa, T., Ohta, Y., Makino, J., Tamura, H., Hojo, Y., Takata, N. & Kawato, S. (2001) *Endocrinology* **142**, 3578–3589.
8. Kawato, S., Hojo, Y. & Kimoto, T. (2002) *Methods Enzymol.* **357**, 241–249.
9. Kawato, S., Yamada, M. & Kimoto, T. (2003) *Adv. Biophys.* **37**, 1–48.
10. Corpéchot, C., Robel, P., Axelson, M., Sjövall, J. & Baulieu, E. E. (1981) *Proc. Natl. Acad. Sci. USA* **78**, 4704–4707.
11. Zwain, I. H. & Yen, S. S. C. (1999) *Endocrinology* **140**, 880–887.
12. Zwain, I. H. & Yen, S. S. C. (1999) *Endocrinology* **140**, 3843–3852.
13. Le Goascogne, C., Sananès, N., Gouézou, M., Takemori, S., Kominami, S., Baulieu, E. E. & Robel, P. (1991) *J. Reprod. Fertil.* **93**, 609–622.
14. Mellon, S. H. & Deschepper, C. F. (1993) *Brain Res.* **629**, 283–292.
15. Baulieu, E. E. & Robel, P. (1998) *Proc. Natl. Acad. Sci. USA* **95**, 4089–4091.
16. Mensah-Nyagan, A. G., Do-Rego, J. L., Beaujean, D., Luu-The, V., Pelletier, G. & Vaudry, H. (1999) *Pharm. Rev.* **51**, 63–81.
17. Wehrenberg, U., Prange-Kiel, J. & Rune, G. M. (2001) *J. Neurochem.* **76**, 1879–1886.
18. Stoffel-Wagner, B., Watzka, M., Schramm, J., Bidlingmaier, F. & Klingmuller, D. (1999) *J. Steroid Biochem. Mol. Biol.* **70**, 237–241.
19. Shinzawa, K., Ishibashi, S., Murakoshi, M., Watanabe, K., Kominami, S., Kawahara, A. & Takemori, S. (1988) *J. Endocrinol.* **119**, 191–200.
20. Jakab, R. L., Horvath, T. L., Leranth, C., Harada, N. & Naftolin, F. (1993) *J. Steroid Biochem. Mol. Biol.* **44**, 481–498.
21. Adams, M. M., Shah, R. A., Janssen, W. G. M. & Morrison, J. H. (2001) *Proc. Natl. Acad. Sci. USA* **98**, 8071–8076.
22. Furukawa, A., Miyatake, A., Ohnishi, T. & Ichikawa, Y. (1998) *J. Neurochem.* **71**, 2231–2238.
23. Ivanova, T. & Beyer, C. (2000) *Cell Tissue Res.* **300**, 231–237.
24. Beyenburg, S., Watzka, M., Blumcke, I., Schramm, J., Bidlingmaier, F., Elger, C. E. & Stoffel-Wagner, B. (2000) *Epilepsy Res.* **41**, 83–91.
25. Pelletier, G., Luu-The, V. & Labrie, F. (1995) *Brain Res.* **704**, 233–239.
26. Melcangi, R. C., Celotti, F., Castano, P. & Martini, L. (1993) *Endocrinology* **132**, 1252–1259.
27. Jellinck, P., Lee, S. J. & McEwen, B. S. (2001) *Steroid Biochem. Mol. Biol.* **78**, 313–317.
28. Rose, K., Stapleton, G., Dott, K., Kieny, M. P., Best, R., Schwarz, M., Russel, D. W., Bjorkhem, I., Seckl, J. & Lathe, R. (1997) *Proc. Natl. Acad. Sci. USA* **94**, 4925–4930.
29. Jung-Testas, I., Hu, Z. Y., Baulieu, E. E. & Robel, P. (1989) *Endocrinology* **125**, 2083–2091.
30. Papadopoulos, V. (1993) *Endocr. Rev.* **14**, 222–240.
31. Compagnone, N. A., Bulfone, A., Rubenstein, J. L. R. & Mellon, S. H. (1995) *Endocrinology* **136**, 5212–5223.
32. Lauber, M. E. & Lichtensteiger, W. (1994) *Endocrinology* **135**, 1661–1668.
33. Woolley, C. S. & McEwen, B. S. (1994) *J. Neurosci.* **14**, 7680–7687.

ELSEVIER

Available online at www.sciencedirect.com

SCIENCE @ DIRECT•

Brain Research 1024 (2004) 233–243

BRAIN RESEARCH

www.elsevier.com/locate/brainres

Research report

A selective increase in phosphorylation of cyclic AMP response element-binding protein in hippocampal CA1 region of male, but not female, rats following contextual fear and passive avoidance conditioning

Koutarou Kudo[a], Chun-Xiang Qiao[a], Shigenobu Kanba[b], Jun Arita[c,*]

[a]*Department of Neuropsychiatry, Interdisciplinary Graduate School of Medicine and Engineering, University of Yamanashi, Tamaho, Yamanashi 409-3898, Japan*
[b]*Department of Neuropsychiatry, Graduate School of Medical Sciences, Kyushu University, Fukuoka 812-8582, Japan*
[c]*Department of Physiology, Interdisciplinary Graduate School of Medicine and Engineering, University of Yamanashi, 1110, Tamaho, Yamanashi 409-3898, Japan*

Accepted 10 August 2004
Available online 12 September 2004

Abstract

Cyclic AMP response element-binding protein (CREB), a transcription factor on which multiple signal transduction pathways converge, has been implicated in long-term memory. We examined whether the sex difference in the performance of contextual fear or passive avoidance conditioning is associated with a change in the activation of CREB in the hippocampus, a neural structure important for long-term memory. The activation of CREB in different subregions within the hippocampus in male and female rats was determined immunohistochemically with an antibody that specifically recognizes the phosphorylated form of CREB (pCREB). With respect to the freezing time in contextual fear conditioning and the step-through latency in passive avoidance conditioning, male rats exhibited better performance than female rats. Phosphorylation of CREB (% pCREB) as revealed by the ratio of the pCREB-immunoreactive (pCREB-ir) cell number to the CREB-immunoreactive cell number was increased in the CA1 region, but not in CA3, CA4, or in the dentate gyrus following training for both types of conditioning in males. In females, such an increase in % pCREB was not found in any hippocampal subregion at any time after conditioning or by increasing the intensity of foot shock. Orchidectomy in males did not alter either the performance of contextual conditioning or conditioning-induced CREB phosphorylation in CA1. The close relationship between behavioral performance and CREB phosphorylation in the CA1 region suggests that hippocampal CREB is involved in the sex difference in some forms of learning and memory.
© 2004 Elsevier B.V. All rights reserved.

Theme: Neural basis of behavior
Topic: Learning and memory: physiology

Keywords: Sex difference; Cyclic AMP response element-binding protein; Hippocampus; Learning; Memory

1. Introduction

An increased intracellular level of the second messenger cyclic AMP after stimulation by hormones and neurotransmitters induces the expression of a variety of genes, indicating an important role of cyclic AMP in protein synthesis. The transcription factor cyclic AMP response element-binding protein (CREB) is activated by cyclic AMP-dependent protein kinase (PKA)-mediated phosphorylation on Ser133 [19] and binds to a consensus DNA sequence termed cyclic AMP response element (CRE) in promoter regions [55], leading to cyclic AMP-regulated expression of the genes for a wide range of proteins such as somatostatin, c-*fos*, brain-derived neurotrophic factor

* Corresponding author. Tel./fax: +81 55 273 6730.
E-mail address: jarita@yamanashi.ac.jp (J. Arita).

0006-8993/$ - see front matter © 2004 Elsevier B.V. All rights reserved.
doi:10.1016/j.brainres.2004.08.007

(BDNF), tissue plasminogen activator, and cyclin proteins [35]. In addition to cyclic AMP/PKA, there are a number of upstream regulators of CREB, including calcium–calmodulin-dependent protein kinase II, protein kinase C, and mitogen-activated protein kinase [46,54], suggesting that CREB is a convergence point of multiple signal transduction pathways.

Learning and memory are integrative brain functions based on neuronal plasticity, which involve a variety of molecules such as neurotransmitters, neurotrophins, and their receptors as well as second messengers and protein kinases. Furthermore, the acquisition and consolidation of long-term, but not short-term, memory depend upon gene expression and protein synthesis [15]. When inhibitors of protein synthesis or mRNA synthesis are administered immediately before or after training, conditioned responses are inhibited at 24 h, but not 1 h, after training in contextual fear conditioning and passive avoidance conditioning, paradigms of fear-motivated learning [1,24,44]. There are several lines of evidence suggesting that CREB plays a key role in long-term memory and synaptic plasticity. First, long-term memory is blocked when CREB production is inhibited by maneuvers of microinjection of the CRE sequence in Aplysia [14], a dominant negative CREB transgene in *Drosophila* [56], and targeted deletion of *CREB* gene in mice [10]. Second, training for contextual fear [25] and passive avoidance conditioning [50] and long-term potentiation (LTP) of synaptic transmission [45], a well-known model for strengthening of synaptic efficacy, are accompanied by spatiotemporal changes in CREB phosphorylation in the hippocampus, a crucial neural structure involved in the acquisition and consolidation of many forms of memory [27,39,48,49].

Sex differences in learning and memory are observed in humans and animals. The presence of sex differences and the predominating sex depend upon learning paradigms. Interestingly, various hippocampal-dependent learning tasks exhibit sex differences: male rats perform better at tasks of contextual fear [2,32] and passive avoidance conditioning [16], whereas female rats perform better at tasks of active avoidance [8,16] and trace eyeblink conditioning [53]. However, the sex difference favoring male rats in the Morris water maze spatial task is not consistent [31]. Furthermore, male rats exhibit greater LTP recorded in the dentate gyrus than do female rats [11,32]. The contribution of gonadal steroid hormones to these sex differences also varies depending upon learning paradigms [52]. However, little is known about the neuroanatomical and biochemical pathways responsible for the sex differences in learning and memory.

In the present study, we addressed the issue of whether the sex differences found in hippocampal-dependent learning paradigms are attributable to differences in the phosphorylation of CREB in the hippocampus. We determined the number of phosphorylated CREB (pCREB)-immunoreactive (ir) cells in hippocampal subregions of male and female rats trained for contextual fear and passive avoidance conditioning. These two learning paradigms were chosen as experimental models because they exhibit prominent sex differences favoring one sex in performance and robust acquisition of memory by a single training session, which enables the detection of a rapid and subtle spatiotemporal change in hippocampal CREB. We demonstrated that the sex differences in these types of hippocampal-dependent conditioning were accompanied by changes in immunoreactive pCREB selectively seen in the CA1 region.

2. Materials and methods

2.1. Animals

Eight-week-old Wistar male rats weighing 240–250 g and female rats weighing 160–170 g were purchased from Japan SLC (Shizuoka, Japan) and were maintained individually in a light/dark cycle-controlled (lights on from 06:00 to 18:00 h) and temperature-controlled animal room with free access to laboratory chow and tap water. Rats were allowed to rest undisturbed in their home cages for at least 5 days prior to conditioning experiments. Because vaginal smears had not been taken, females killed after conditioning were not at a specific stage but at random stages of the estrous cycle. All experimental procedures were conducted in accordance with the guidelines of the Ethical Committee of Animal Experiments at the University of Yamanashi. All efforts were made to minimize the number of animals used and their suffering.

2.2. Contextual fear conditioning

A contextual fear-conditioning task was performed in a conditioning chamber placed in a sound-attenuating box during the light phase of the cycle. The conditioning chamber (28 W×21 H×22 D cm^3) was constructed of clear Plexiglas on the top and four sides. The floor of the chamber was lined with 18 stainless steel bars (4 mm in diameter; 1.5 cm spacing), which formed a foot shock grid to deliver scrambled shocks produced by a stimulator (SS-104J Nihon Koden, Tokyo, Japan). The foot shock was a 2-s direct current of 0.75 mA, and served as the aversive unconditioned stimulus (US). Between training and testing sessions, the floor and interior of the conditioning chamber were cleaned with a 75% ethanol solution. The sound-attenuating box (48 W×48 H×48 D cm^3) was provided with a 20-W houselight and a ventilation fan located at the top of the box, supplying background white noise (74 dB). Because hippocampal lesions have been reported to disrupt freezing to a context when an explicit cue is paired with foot shock in that context (background contextual fear conditioning), but have no effect when a context is paired directly with shock (foreground contextual fear conditioning) [40], a discrete tone-conditioned stimulus (CS) was given on

general contextual stimuli. The tone (800 Hz, 20-s duration, 80 dB) was delivered by two speakers located in the lower corner of the sound-attenuating box. Prior to training, rats received 3-day habituation, in which they were placed in the conditioning chamber for 1 s and then returned to their home cage, once a day. On the day of training, the rats were placed in the conditioning chamber and allowed to explore for 3 min. A foot shock was delivered three times at 1, 9, and 18 s after the onset of the tone CS. The rats were then allowed to recover for 30 s in the conditioning chamber and returned to their home cage. An hour later, the rats were again introduced into the conditioning chamber in which they had been trained and were tested for a 5-min period, during which no tone CS was presented. In time course studies, the rats were tested at varying times of 1–24 h after training. Conditioning was assessed by measuring the time spent freezing for each 30 s during the testing period. Freezing behavior was defined as cessation of all but respiratory movement. Data were quantified and presented as the percentage of total freezing time in the 5-min testing period.

2.3. Passive avoidance conditioning

A passive avoidance-conditioning task was performed using a step-through type of conditioning chamber during the dark phase of the cycle. The conditioning chamber was divided into two sections, one light and one dark, by a partition with a closable trap door (light section, 20 W×40 H×20 D cm^3; dark section, 20 W×40 H×15 D cm^3). The light section was illuminated by a 20-W houselight placed on the top of the light section. Both the sections had a 17-bar (4 mm in diameter, 1 cm spacing) foot shock grid floor. The bars in the dark section were connected to a stimulator to deliver scrambled shocks. On days 1 and 2 of the experiment, rats received acclimatization trials, in which they were placed in the light section and allowed to move freely to the dark section. Immediately after the entire body of the rat was within the dark section (defined as step-through), the trap door was closed. After 2 min, the rats were removed from the chamber and returned to their home cage. This acclimatization trial was performed twice each day with a 3-min interval. After two consecutive acclimatization trials on day 2, the rats were placed in the light section for training, and a foot shock (1-s duration, 0.6 mA) was delivered immediately after step-through. The rats was allowed to recover for 2 min in the dark section and then returned to their home cage. Thirty minutes later, the rats were placed in the light section and tested for step-through. The latency for step-through was measured during a maximum testing period of 5 min.

2.4. Immunohistochemistry

Rats were decapitated immediately after completion of testing. Brains were removed within 90 s, frozen rapidly in dry ice-isopentane, and stored at −70 °C until sections were made. About 10-μm-thick coronal sections were cut using a cryostat with reference to the atlas of Paxinos and Watson [38]. Hippocampal sections located 2.9 mm posterior to the bregma suture were placed on 3-aminopropyltriethoxysilane-coated glass slides (Matsunami Glass, Osaka, Japan). The hippocampal sections were fixed with 4% paraformaldehyde in 0.1 M phosphate buffer, pH 7.0 for 15 min and washed twice in 0.01 M phosphate-buffered saline, pH 7.4 for 10 min each. The sections were then dehydrated with a graded series of 70%, 95%, and 100% ethanol, and rehydrated with a reversed series of the same ethanol concentrations, which was shown in a preliminary experiment to be effective in decreasing background staining. The sections were stored at −20 °C in a cryoprotectant (25% ethylene glycol, 25% glycerin in 0.05 M phosphate buffer) until immunostaining. The sections were treated with 3% H_2O_2 in phosphate-buffered saline for 10 min to block endogenous peroxidase activity and with 10% normal horse serum in Tris-buffered saline, pH 7.4 (TBS) for 30 min to block nonspecific staining. The sections were thereafter immunostained with either anti-pCREB antibody at 1:500 dilution (Cell Signaling Technology, Beverly, MA), which specifically recognizes CREB phosphorylated at Ser133, or anti-CREB antibody, which detects both the phosphorylated and unphosphorylated forms of CREB, at 1:2000 dilution in TBS containing 10% normal horse serum at 4 °C for 48 h. The immunoreactive specificity was confirmed by the result that no staining in hippocampal tissue was found with omission of the primary antibodies. Tissue sections were incubated with biotinylated anti-rabbit IgG (Vector, Burlingame, CA) at 1:200 dilution in TBS containing 10% normal

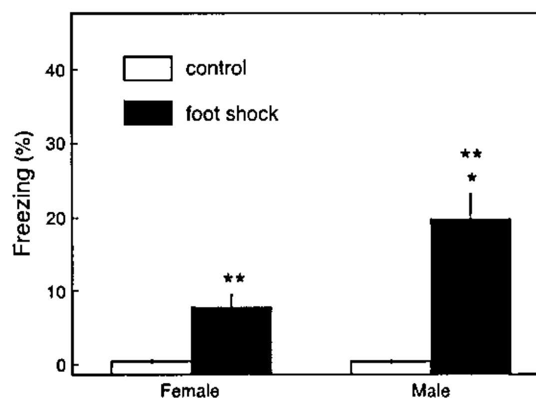

Fig. 1. Freezing after contextual fear conditioning in male and randomly cycling female rats. During training, male and female rats received a foot shock (0.75 mA) while control rats received the same training procedures but without the foot shock. One hour after training, they were tested for freezing behavior. Freezing is expressed as the percentage of the time spent in freezing in a total 5-min testing time. Each bar indicates mean±S.E.M. The numbers of animals are 6 and 5 for control and foot-shocked female groups, and 7 and 7 for control and foot-shocked male groups, respectively. *Significantly different from foot-shocked females; **significantly different from controls at $p<0.05$.

horse serum for 1 h followed by avidin-biotinylated horse-radish peroxidase complex (Vectastain Elite ABC kit, Vector) in TBS for 1 h. Between incubations, the sections were washed three times for 7 min each in TBS containing 0.3% Tween 20. Peroxidase reaction was performed for 10 min using a DAB Peroxidase Substrate Tablet Set (Sigma, St. Louis, MO) in the presence of 1% nickel ammonium sulfate. The sections were dehydrated with ethanol, cleared with xylene, and were coverslipped with Histomount (Zymed, San Francisco, CA).

Microscopic images of randomized sections were captured into a computer with a high-sensitivity CCD camera (DP-50, Olympus, Tokyo, Japan). Every cell, located within an 800×600 μm^2 area, in the pyramidal cell layers of CA1, CA3, and CA4 and in the granule cell layer of the inferior blade of the dentate gyrus was subjected to assessment of immunoreactivity by an investigator who did not have information on the sections. Neurons were judged to be immunoreactive and counted when their nuclei were stained as intensely as those seen within several inner lines of the

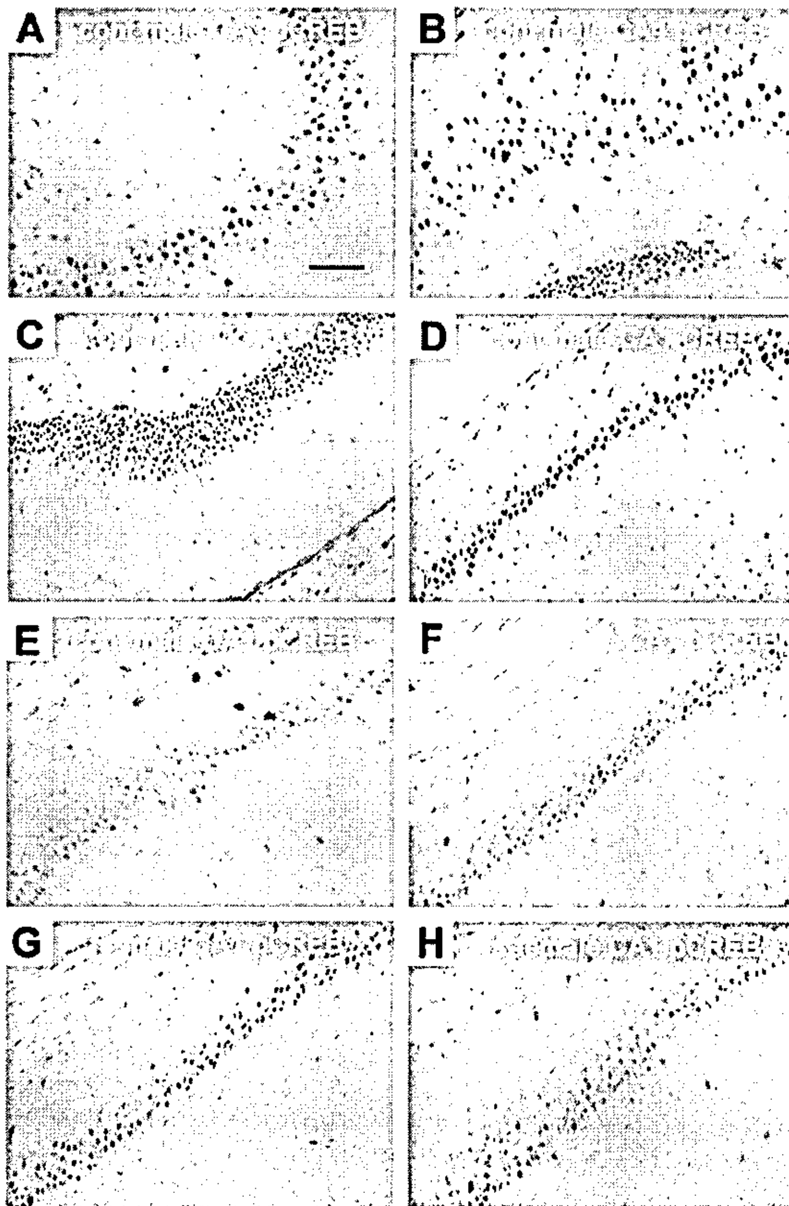

Fig. 2. Photomicrographs showing hippocampal pCREB-ir cells after contextual fear conditioning in male and female rats. During training, male and female rats received a foot shock while control rats received the same training procedures but without the foot shock. One hour after training, they were tested for freezing behavior and then killed for immunohistochemical staining for pCREB and CREB in hippocampal subregions. pCREB-ir cells in CA3 (A), CA4 (B), and dentate gyrus (C) and CREB-ir cells in CA1 (D) in a control male rat. pCREB-ir cells in CA1 in a control male (E), control female (F), foot-shocked (fs) male (G), and fs female rat (H). Scale bar, 100 μm.

granule cell layer in the dentate gyrus. Two independent counts were made from at least two different sections per animal and averaged.

2.5. Statistical analysis

The experimental data were analyzed by nonparametric analysis of Kruskal–Wallis for multiple comparison. Comparisons between pairs of groups were carried out by Mann–Whitney U-test based on the Bonferroni correction. Differences at $p<0.05$ were considered statistically significant.

3. Results

3.1. Freezing and number of hippocampal pCREB-ir cells after contextual fear conditioning in male and female rats

Control rats that had not received foot shock during training exhibited little or no freezing behavior in response to the context during testing. There was no significant difference in freezing between control male (n=7) and female rats (n=6; Fig. 1). Although both male (n=7) and female rats (n=5) that had received a foot shock with an intensity of 0.75 mA exhibited conditional freezing after 1 h (χ^2=18.9, df=3, $p<0.0001$), freezing was 2.6-fold longer in males than in females (p=0.006).

When the hippocampus from these rats was immunostained using an antibody that specifically recognizes pCREB, numerous intensely immunostained cells were observed in hippocampal subregions including CA3 (Fig. 2A), CA4 (Fig. 2B), and the dentate gyrus in control rats (Fig. 2C). In contrast to these subregions, CA1 contained a marked smaller number of pCREB-ir cells (Fig. 2E and F). No apparent sex difference existed in the distribution of pCREB-ir cells within the hippocampus in control rats. The majority of cells in the granule and pyramidal cell layers of these hippocampal subregions exhibited intense immunoreactivity when stained with a CREB-specific antibody (Fig. 2D). Comparison of adjacent hippocampal sections that were immunostained with pCREB and CREB antibodies revealed that CREB was strongly phosphorylated in many CREB-ir cells in hippocampal subregions except CA1 under control conditions (data not shown). Taking the possibility of variations in the cell density or cell number in hippocampal sections between the sexes into consideration [29,43], we chose the ratio of the pCREB-ir cell number counted in a given area of a section to the CREB-ir cell number in the corresponding area of the adjacent section (% pCREB-ir cell number), rather than the absolute cell number, as a measure of CREB phosphorylation, to minimize the variations. The range of % pCREB-ir cell number was 75–95% in CA3, CA4, and the dentate gyrus in control male and female rats, while it was less than 20% in CA1 (Fig. 3).

In males, the % pCREB-ir cell number was not affected at 1 h after foot shock in any of the CA3, CA4, and dentate

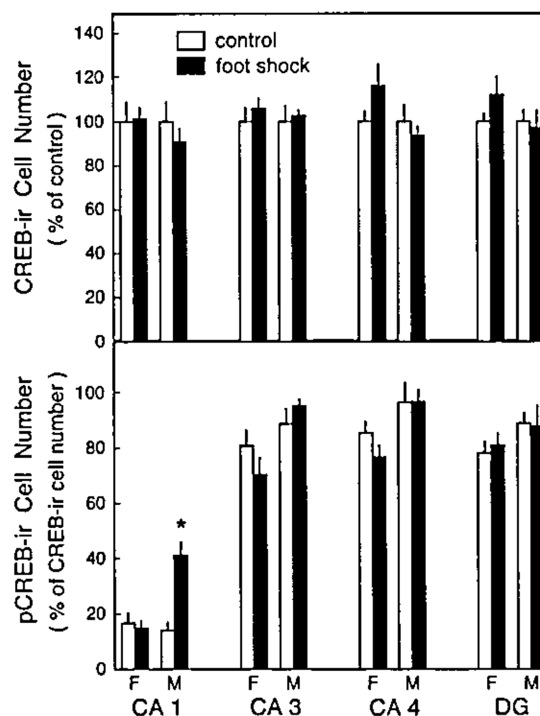

Fig. 3. Numbers of hippocampal CREB- and pCREB-ir cells immediately after contextual fear conditioning in male and randomly cycling female rats. During training, male and female rats received a foot shock (0.75 mA), while control rats received the same training procedures but without the foot shock. One hour after training, they were tested for freezing behavior and then killed for immunohistochemical staining for CREB and pCREB in hippocampal subregions. CREB-ir cell number (upper panel) is defined as the percentage of the CREB-ir cell number in each subregion in control rats. pCREB-ir cell number (lower panel) is defined as the percentage of the pCREB-ir cell number to the CREB-ir cell number counted in adjacent sections in the same subregions. Each bar indicates mean±S.E.M. The numbers of animal are 6 and 5 for control and foot-shocked female groups, and 7 and 7 for control and foot-shocked male groups, respectively. *Significantly different from controls at $p<0.05$. Abbreviations: F, females; M, males; DG, dentate gyrus.

gyrus subregions, but was markedly increased in CA1 (χ^2=13.3, df=3, p=0.004; Figs. 2G and 3, lower panel), while the number of CREB-ir cells exhibited no change after foot shock in any hippocampal subregion (Fig. 3, upper panel). In females, there was no significant change in the numbers of pCREB- and CREB-ir cells in any subregion after foot shock (Fig. 2H), leading to a significantly lower % pCREB-ir cell number in CA1 compared to that in males (p=0.001).

3.2. Time course of freezing and number of hippocampal pCREB-ir cells following contextual fear conditioning in male and female rats

To test whether an increased % pCREB-ir cell number in CA1, as observed 1 h after foot shock in males is maintained thereafter in males and whether it occurs at different time points in females, freezing and the number of hippocampal

pCREB-ir cells were determined at various times after foot shock (each time point group consists of 5–6 animals). Significantly longer freezing was found not only at 1 h but also during a period of 5–24 h after a 0.75-mA foot shock in males compared to that in control males (χ^2=36.8, df=7, p<0.0001; Fig. 4, upper left panel). Although % pCREB-ir cell number in CA1 was increased 1 h after foot shock and maintained thereafter at similar levels (χ^2=28.3, df=7, p<0.0001), statistically significant differences between the control and trained rats were found only at 1 and 5 h (p=0.002; Fig. 4, lower left panel). In trained females, the slight but significant increase in freezing observed 1 h after foot shock was maintained consistently at all time points of 5–24 h (Fig. 4, upper right panel). Unlike in males, % pCREB-ir cell number in CA1 did not differ between trained and control female rats, at least at the time points examined (Fig. 4, lower right panel). % pCREB-ir cell number in hippocampal subregions other than CA1 did not show any difference between control and trained rats at all time points regardless of the sex (data not shown).

3.3. Effects of increasing foot shock intensity on freezing and number of hippocampal pCREB-ir cells in female rats

Because shorter freezing and the absence of an increase in % pCREB-ir cell number in CA1 following conditioning in females raised the possibility that these sex differences might be due to low sensitivity to foot shock in females, the effects of increased intensity of foot shock on freezing and % pCREB-ir cell number were examined (each intensity group consists of six animals). In females, a foot shock with an intensity of 0.75 mA induced significant freezing 1 h later (p=0.003) as observed in Figs. 1 and 4 (Fig. 5, upper panel). The freezing induced by foot shock tended to increase with an increase in the intensity of foot shock from 0.75 to 1.2 mA, but this rise was not statistically significant (p=0.18). No significant change in % pCREB-ir cell number in CA1 was seen even after increasing the intensity of foot shock (χ^2=1.9, df=3, p=0.60; Fig. 5, lower panel).

3.4. Effects of orchidectomy on freezing and number of hippocampal pCREB-ir cells following contextual fear conditioning in male rats

To test whether the male-specific increase in % pCREB-ir cell number in CA1 following conditioning is dependent on circulating testosterone, % pCREB-ir cell number was compared in sham-operated and orchidectomized male rats (each group consists of 6 animals). Orchidectomy affected neither freezing at 1 h after 0.75 mA foot shock (Fig. 6, upper panel) nor % pCREB-ir cell number in all hippocampal subregions including CA1 (Fig. 6, lower panel).

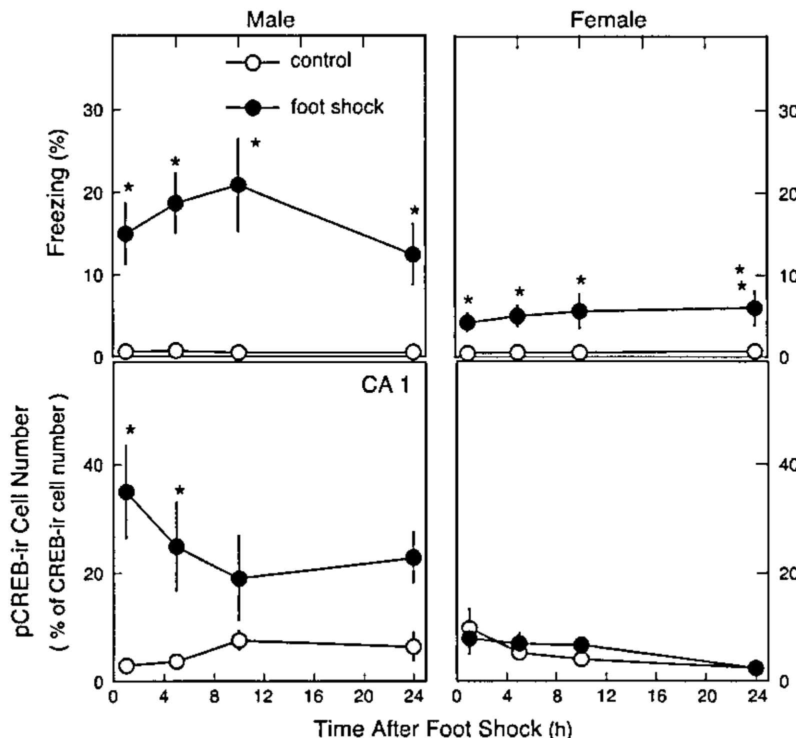

Fig. 4. Time course of freezing and number of CA1 pCREB-ir cells following contextual fear conditioning in male and female rats. Male (left panels) and female rats (right panels) that had received either a foot shock (●; 0.75 mA) or no shock as controls (O) were tested for freezing behavior at various time points after training (upper panels). Immediately after testing, the rats were killed for immunohistochemical staining for pCREB in the CA1 region (lower panels). pCREB-ir cell number is defined in the legend of Fig. 3. Each bar indicates mean±S.E.M. of 5–6 animals. *Significantly different from controls without foot shock at p<0.05.

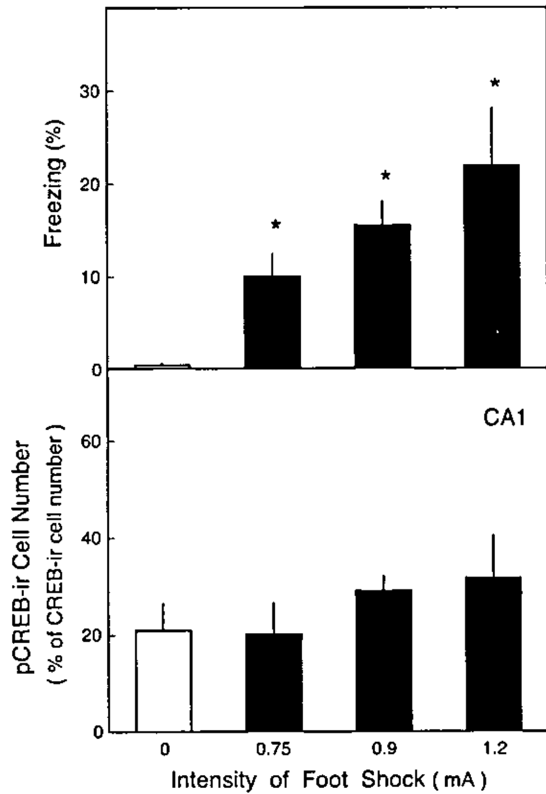

Fig. 5. Effects of increasing foot shock intensity on freezing and number of CA1 pCREB-ir cells in female rats. Female rats that had received a foot shock of various intensity were tested for freezing behavior 1 h after training (upper panel). Immediately after testing, the rats were killed for immunohistochemical staining for pCREB in CA1 (lower panel). pCREB-ir cell number is defined in the legend of Fig. 3. Each bar indicates mean±S.E.M. of six animals. *Significantly different from controls without foot shock at $p<0.05$.

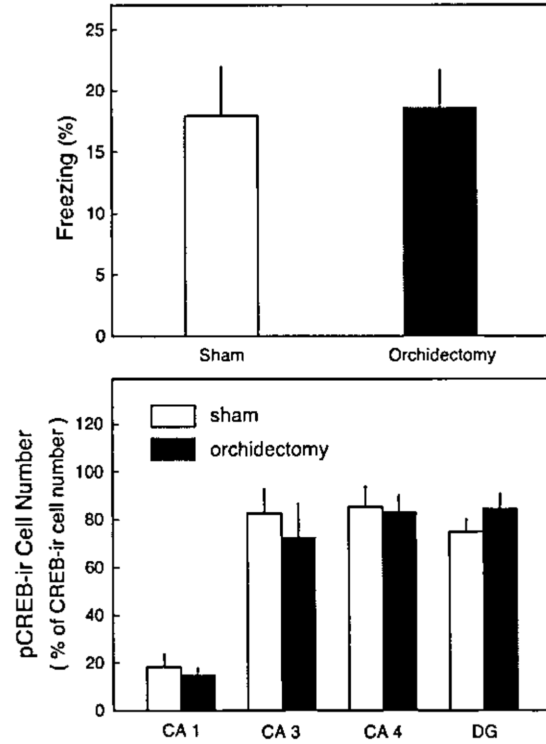

Fig. 6. Effects of orchidectomy on freezing and number of hippocampal pCREB-ir cells following contextual fear conditioning in male rats. Sham-operated and orchidectomized male rats that had received a foot shock (0.75 mA) were tested for freezing behavior 1 h after training (upper panel). Immediately after testing, the rats were killed for immunohistochemical staining for pCREB in hippocampal subregions (lower panel). pCREB-ir cell number is defined in the legend of Fig. 3. Each bar indicates mean±S.E.M. of six animals.

3.5. Step-through latency and number of hippocampal pCREB-ir cells after passive avoidance conditioning in male and female rats

To extend our results of the sex differences obtained in experiments using contextual fear conditioning, behavioral performance and % pCREB-ir cell number in hippocampal subregions were examined in males and females trained for passive avoidance conditioning, another hippocampal-dependent conditioning paradigm that shows a sex difference [16,52]. Control male (n=6) and female rats (n=6) stepped through to the dark section of the conditioning chamber during testing, with similar low step-through latencies (Fig. 7). A foot shock of 0.6 mA increased the step-through latency 12-fold above the control level 30 min later in male rats (n=7, χ^2=12.3, df=3, p=0.006), while there was no significant increase in this measure in female rats (n=7). Male and female control rats exhibited similar % pCREB-ir cell numbers in all hippocampal subregions except CA1, in which % pCREB-ir cell number was significantly higher in males than in females (χ^2=19.1,

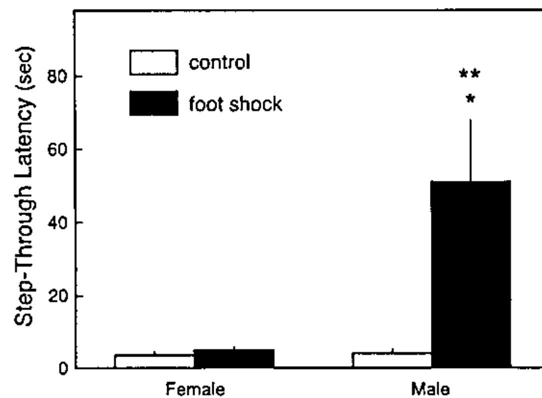

Fig. 7. Step-through latency after passive avoidance conditioning in male and female rats. During training, male and female rats received a foot shock (0.6 mA) in the dark section of a conditioning chamber while control rats received the same training procedures but without the foot shock. Thirty minutes after training, they were tested for stepping through to the dark section. Each bar indicates mean±S.E.M. The numbers of animals are 6 and 7 for control and foot-shocked female groups, and 6 and 7 for control and foot-shocked male groups, respectively. *Significantly different from foot-shocked females; **significantly different from controls at $p<0.05$.

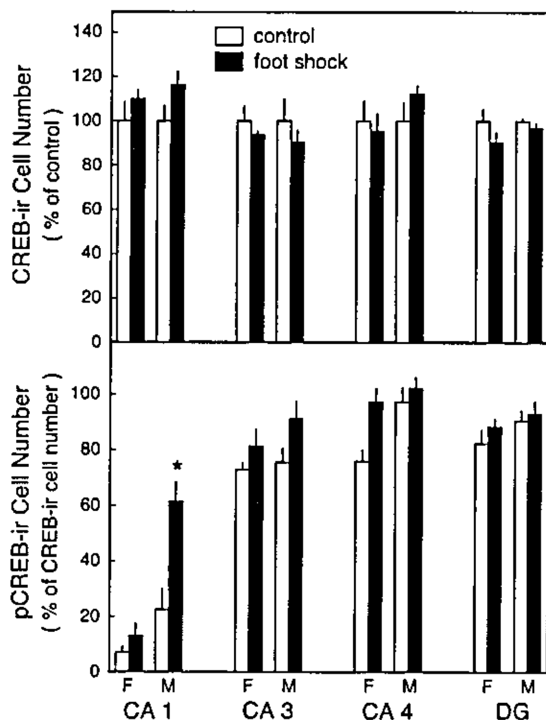

Fig. 8. Numbers of hippocampal CREB- and pCREB-ir cells after passive avoidance conditioning in male and randomly cycling female rats. During training, male and female rats received a foot shock (0.6 mA) in the dark section of a conditioning chamber while control rats received the same training procedures but without the foot shock. Thirty minutes after training, they were tested for stepping through to the dark section and killed for immunohistochemical staining for CREB (upper panel) and pCREB (lower panel) in hippocampal subregions. pCREB-ir cell number is defined in the legend of Fig. 3. Each bar indicates mean±S.E.M. The numbers of animals are 6 and 7 for control and foot-shocked female groups, and 6 and 7 for control and foot-shocked male groups, respectively. *Significantly different from controls at $p<0.05$. Abbreviations: F, females; M, males; DG, dentate gyrus.

df=3, $p<0.0001$; Fig. 8, lower panel). After passive avoidance conditioning, there was a marked sex difference in % pCREB-ir cell number in the hippocampus, which was virtually the same as that observed in contextual fear conditioning (χ^2=19.4, df=3, $p<0.0001$): % pCREB-ir cell number rose 2.7-fold above the control level only in CA1 in trained male rats (p=0.001), while there was no change in % pCREB-ir cell number in any hippocampal subregion in trained female rats. There was no change in number of CREB-ir cells in any of the hippocampal regions following conditioning (Fig. 8, upper panel).

4. Discussion

To determine dynamic spatiotemporal changes in hippocampal CREB activation following conditioning, we assessed the number of pCREB-ir neurons in frozen sections immunohistochemically using a phospho-specific CREB antibody. Our immunohistochemical analysis revealed that in control rats that received no foot shock, most of the CREB-ir neurons were also immunoreactive for pCREB in all hippocampal subregions and many other brain areas examined except CA1. It remains to be elucidated how the notably low pCREB levels in CA1 under basal conditions are related to a selective increase in pCREB following conditioning in this area (discussed below) and the acquisition and consolidation of memory. Following both tasks of contextual fear and passive avoidance conditioning, the number of pCREB-ir neurons was increased selectively in CA1 but not in other hippocampal subregions CA3, CA4, and the dentate gyrus in male rats. There was no change in the number of CREB-ir cells in CA1, suggesting that the increase in pCREB-ir cell number is due to increased phosphorylation of CREB. Our results on the hippocampal distribution of pCREB-ir neurons in males following conditioning are consistent with those by Impey et al. [25], showing that CRE-lacZ gene expression was increased in CA1 and CA3 following contextual fear and passive avoidance conditioning, while an increase in pCREB was found specifically in CA1 after contextual fear conditioning in mice. However, Taubenfeld et al. [50] reported that, in male rats, passive avoidance conditioning induced an increase in pCREB-ir neurons in the dentate gyrus and CA3 in addition to CA1. The discrepancy in the distribution of pCREB-ir neurons between their studies and ours is difficult to explain at present. We chose to use freshly frozen brains for immunostaining because a preliminary experiment has shown a marked reduction of pCREB immunoreactivity in the dentate gyrus and CA regions by transcardiac perfusion with a fixative under anesthesia. Such rapid dephosphorylation of pCREB in the hippocampus might have caused a difference in the detectable amount of pCREB in different histological preparations. Our results do not completely exclude the possibility of a simultaneous increase in pCREB in other areas of the hippocampus after conditioning in male rats. In contrast to CA1, in which undetectable pCREB levels in most cells before conditioning make it easy to detect an increase in pCREB after conditioning, a semiquantitative histochemical analysis based on a parameter of the immunoreactive cell number may mask an additional increase in amounts of pCREB after conditioning in the dentate gyrus and CA3, in which most cells are immunoreactive for pCREB before conditioning. Although the distribution of pCREB-ir neurons in the male hippocampus after conditioning differs somewhat between these two studies, the results in these studies that an increase in pCREB was consistently found in CA1 after both conditioning paradigms emphasize an important role of phosphorylation and activation of CREB in CA1 in emotional learning and memory in males. The specific importance of CA1 in the conditioning paradigms used in the present study has been demonstrated by several studies. Passive avoidance conditioning is impaired in carbon monoxide-induced amnesia [36] and transient ischemia models [4] which selectively damage neurons in

CA1. Furthermore, contextual fear conditioning has recently been shown to be disrupted in CA1-specific *N*-methyl-D-aspartate receptor1-knockout mice [42].

For contextual fear conditioning, males rats exhibited more freezing behavior both at 1 h and later time points 5–24 h after conditioning than did female rats. Because conditioned responses tested at these time points reflect short- and long-term memories, respectively, these results suggest that there is a sex difference in short-term memory obtained by contextual fear conditioning in addition to that in long-term memory as shown by other studies [2,30]. Consistent with this view is our result that step-through latencies, as early as 30 min after passive avoidance conditioning, were higher in males than in females. In the present study, CA1, the sole hippocampal subregion in which the number of pCREB-ir neurons was increased after the two conditioning paradigms in males, also exhibited marked sex differences in CREB phosphorylation; in females, the number of pCREB-ir neurons in this area was not altered at any time after conditioning or by any increase in intensity of foot shock. The positive correlation between pCREB-ir neurons in CA1 and behavioral performance in males and females suggests that a difference in CREB activation is involved in the sex differences in contextual fear and passive avoidance conditioning. Although it is evident that there is a sex difference at the level of CREB phosphorylation itself, it is unknown at present whether a sex difference at some level upstream of CREB is responsible for the difference in CREB phosphorylation. Because calcium–calmodulin-dependent protein kinase II [46] and the mitogen-activated protein kinase cascade [54] regulate the activity of CREB and have been implicated in hippocampal-dependent learning and memory [6,47], the function and regulation of these CREB-upstream regulators in CA1 neurons may differ between the sexes, leading to the sex difference in CREB phosphorylation. Alternatively, a sex difference may exist in neurons that send nerve fibers directly to CA1 neurons such as hippocampal intrinsic neurons in the dentate gyrus and CA3 or in extrinsic neurons, leading to a transsynaptic modification of CREB phosphorylation in CA1. Indeed, consistent with this idea is the finding of Maren et al. [30] that the sex difference in contextual fear conditioning was correlated with that in LTP recorded in the dentate gyrus. Furthermore, neuroanatomical studies have demonstrated that sex differences exist in dendritic density, synaptic connectivity, cell number, and cell layer width in hippocampal subregions other than CA1 [26,29,33,43]. Thus, it remains to be clarified whether there is a sex difference at levels upstream of CREB and what upstream signaling molecules or neurons are involved in the sex differences in behavioral performance.

We postulate that CREB activation and phosphorylation found within 1 h after training contribute to freezing behavior occurring at later times; based on the findings by Bourtchaladze et al. [10] that in mice with targeted disruption of CREB, freezing was decreased at 24 h but not at 30 min after training. This is consistent with the time-dependent effect of protein synthesis blockers; treatment with the blockers 30 min before or immediately after training suppresses freezing at 24 h, but the blockers are not effective when given at 1 h after training, suggesting that only a single short wave of protein synthesis during or immediately after training is required for contextual fear conditioning over 24 h [1]. There are many proteins whose expressions are directed by the CREB–CRE transcriptional pathway and that have been implicated in the formation of multiple types of memory. One of the best studied molecules that likely mediate the CREB action is BDNF, which has been shown to be involved in synaptic plasticity and long-term memory formation as well as the differentiation and survival of neurons [41]. In the CA1 region, LTP is enhanced by BDNF [17], reduced by BDNF antibody [12] or targeted deletion of the *BDNF* gene [28], and associated with increased expression of BDNF mRNA [37]. Recently, rapid and selective induction of BDNF expression has been shown to occur in CA1 after contextual fear conditioning [22]. In this regard, it would be of interest to determine whether males and females exhibit a difference in BDNF expression in CA1 after the conditioning paradigms used in the present study.

Although we demonstrated a close relationship between sex differences in behavioral performance and CA1 pCREB level, the exact neural role of CREB phosphorylation in CA1 in the sexually dimorphic conditioning tasks remains unknown. Although the role of the hippocampus in contextual fear conditioning has been poorly understood and controversial [48], Anagnostaras et al. [3] have proposed that its specific role is the construction and temporary maintenance of a unified representation of a contextual CS, rather than the CS–US association or shock US representation. On the other hand, CREB has been shown to be involved in a variety of learning paradigms in a wide range of species [10,14,56] and in LTP [10,45]. Taking these results together, we prefer to postulate that the sex difference in CREB phosphorylation in CA1 reflects a difference in the learning process itself. This idea is supported by the fact that similar changes in CREB phosphorylation were observed in CA1 following two different learning paradigms of contextual fear and passive avoidance conditioning. However, our results, nonetheless, may be open to an alternative interpretation supported by several lines of evidence. First, at least with regard to passive avoidance conditioning, it has been suggested that the sex difference in performance is attributable not to differences in learning capacity [51], but to differences in locomotor activity between the sexes [23]; females are generally more active than males in open-field tests [7], and the open-field activity is reduced to a greater extent in males than in females after foot shock [23], raising the possibility that the reduced locomotor activity leads to a greater step-through latency in passive avoidance conditioning in males. Second, based on the findings that hippocampal lesions caused increased locomotor activity [9,20], which might interfere with freezing, and disrupted fear-conditioned

freezing but not fear-potentiated startle [34], it has been proposed that the hippocampus is merely involved in behavioral inhibition but is not essential for contextual fear itself. Third, Archer [5] has suggested that male and female rats exhibit different responses to fear stimuli, with males tending to perform an inactive response, e.g., freezing, and females tending to perform an active response, e.g., escaping. Taking these results together, it cannot be completely excluded that the sex difference in pCREB in CA1 observed in the present study reflects a sex difference in the hippocampal dependency of different conditional responses that males and females exhibit. Further studies are needed to determine whether, in females, CREB is activated by conditioning in another brain area such as the amygdala, a major neural structure that is involved in contextual fear conditioning.

Anagnostaras et al. [2] reported that orchidectomy had no effect on the performance of contextual fear conditioning in males. In agreement with their results, we found that orchidectomy affected neither the performance of contextual fear conditioning nor pCREB-ir cell number in CA1 following conditioning in males. These results indicate that the male-specific increase in the number of CA1 pCREB-ir cells following contextual fear conditioning is independent of the activational action of steroid hormones secreted from the testis in adulthood. In females, the performance of contextual fear conditioning is altered during the estrous cycle and by ovariectomy [21,32]. Furthermore, hippocampal LTP, which is also accompanied by changes in CREB phosphorylation [45], is modulated by estrogen [13,18,21]. Despite the prominent effects of estrogen shown in these studies, the present study demonstrates a significant difference in conditioning performance between randomly cycling females and males, suggesting that the estrous cycle-associated changes in performance in females are less marked than its sex difference. The mechanism of the formation of the sex differences in contextual fear conditioning and CREB phosphorylation in CA1 remains to be clarified. Because many of the sex differences in other hippocampal-dependent learning paradigms are determined by perinatal testosterone secreted from the testis [26,43,52], it seems likely that the neural structure underlying the sex differences in contextual fear conditioning and CREB phosphorylation undergoes sexual differentiation under the organizational action of testosterone early in development. This idea is supported by the neuroanatomical finding that treatment of neonatal females with testosterone masculinized the CA1 pyramidal cell field volume and neuronal soma size [26].

Acknowledgements

This work was supported in part by the Ministry of Education, Science, and Culture of Japan (Grant-in-Aid for Scientific Research, 15590206).

References

[1] T. Abel, P.V. Nguyen, M. Barad, T.A.S. Deuel, E.R. Kandel, R. Bourtchouladze, Genetic demonstration of a role for PKA in the late phase of LTP and in hippocampus-based long-term memory, Cell 88 (1997) 615–626.

[2] S.G. Anagnostaras, S. Maren, J.P. DeCola, N.I. Lane, G.D. Gale, B.A. Schlinger, M.S. Fanselow, Testicular hormones do not regulate sexually dimorphic Pavlovian fear conditioning or perforant-path long-term potentiation in adult male rats, Behav. Brain Res. 92 (1998) 1–9.

[3] S.G. Anagnostaras, G.D. Gale, M.S. Fanselow, Hippocampus and contextual fear conditioning: recent controversies and advances, Hippocampus 11 (2001) 8–17.

[4] H. Araki, M. Nojiri, K. Kawashima, M. Kimura, H. Aihara, Behavioral, electroencephalographic and histopathological studies on Mongolian gerbils with occluded common carotid arteries, Physiol. Behav. 38 (1986) 89–94.

[5] J. Archer, Rodent sex differences in emotional and related behavior, Behav. Biol. 14 (1975) 459–479.

[6] C.M. Atkins, J.C. Selcher, J.J. Petraitis, J.M. Trzaskos, J.D. Sweatt, The MAPK cascade is required for mammalian associative learning, Nat. Neurosci. 1 (1998) 602–609.

[7] W.W. Beatty, Gonadal hormones and sex differences in nonreproductive behaviors in rodents: organizational and activational influences, Horm. Behav. 12 (1979) 112–163.

[8] W.W. Beatty, P.A. Beatty, Hormonal determinants of sex differences in avoidance behavior and reactivity to electric shock in the rat, J. Comp. Physiol. Psychol. 73 (1970) 446–455.

[9] D.C. Blanchard, R.J. Blanchard, M.C. Lee, K.K. Fukunaga, Movement arrest and the hippocampus, Physiol. Psychol. 5 (1977) 331–335.

[10] R. Bourtchuladze, B. Frenguelli, J. Blendy, D. Cioffi, G. Schutz, A.J. Silva, Deficient long-term memory in mice with a targeted mutation of the cAMP-responsive element-binding protein, Cell 79 (1994) 59–68.

[11] J.D. Bronzino, P. Kehoe, R.J. Austin-LaFrance, R.J. Rushmore, J. Kurdian, Neonatal isolation alters LTP in freely moving juvenile rats: sex differences, Brain Res. Bull. 41 (1996) 175–183.

[12] G. Chen, R. Kolbeck, Y. Barde, T. Bonhoeffer, A. Kossel, Relative contribution of endogenous neurotrophins in hippocampal long-term potentiation, J. Neurosci. 19 (1999) 7983–7990.

[13] D.A. Córdoba-Montoya, H.F. Carrer, Estrogen facilitates induction of long term potentiation in the hippocampus of awake rats, Brain Res. 778 (1997) 430–438.

[14] P.K. Dash, B. Hochner, E.R. Kandel, Injection of the cAMP-responsive element into the nucleus to Aplysia sensory neurons blocks long-term facilitation, Nature 345 (1990) 718–721.

[15] H.P. Davis, L.R. Squire, Protein synthesis and memory: a review, Psychol. Bull. 96 (1984) 518–559.

[16] A. Denti, A. Epstein, Sex differences in the acquisition of two kinds of avoidance behavior in rats, Physiol. Behav. 8 (1972) 611–615.

[17] A. Figurov, L.D. Pozzo-Miller, P. Olafsson, T. Wang, B. Lu, Regulation of synaptic responses to high-frequency stimulation and LTP by neurotrophins in the hippocampus, Nature 381 (1996) 706–709.

[18] M.R. Foy, J. Xu, X. Xie, R.D. Brinton, R.F. Thompson, T.W. Berger, 17β-estradiol enhances NMDA receptor-mediated EPSPs and long-term potentiation, J. Neurophysiol. 81 (1999) 925–929.

[19] G.A. Gonzalez, M.R. Montminy, Cyclic AMP stimulates somatostatin gene transcription by phosphorylation of CREB at serine 133, Cell 59 (1989) 675–680.

[20] M. Good, R.C. Honey, Dissociable effects of selective lesions to hippocampal subsystems on exploratory behavior, contextual learning, and spatial learning, Behav. Neurosci. 111 (1997) 487–493.

[21] R.R. Gupta, S. Sen, L.L. Diepenhorst, C.N. Rudick, S. Maren, Estrogen modulates sexually dimorphic contextual fear conditioning

and hippocampal long-term potentiation (LTP) in rats, Brain Res. 888 (2001) 356–365.
[22] J. Hall, K.L. Thomas, B.J. Everitt, Rapid and selective induction of BDNF expression in the hippocampus during contextual learning, Nat. Neurosci. 3 (2000) 533–535.
[23] R.P.W. Heinsbroek, F. van Haaren, N.E. van de Poll, Sex differences in passive avoidance behavior of rats: sex-dependent susceptibility to shock-induced behavioral depression, Physiol. Behav. 43 (1988) 201–206.
[24] L.M. Igaz, M.R.M. Vianna, J.H. Medina, I. Izquierdo, Two time periods of hippocampal mRNA synthesis are required for memory consolidation of fear-motivated learning, J. Neurosci. 22 (2002) 6781–6789.
[25] S. Impey, D.M. Smith, K. Obrietan, R. Donahue, C. Wade, D.R. Storm, Stimulation of cAMP response element (CRE)-mediated transcription during contextual learning, Nat. Neurosci. 1 (1998) 595–601.
[26] C. Isogor, D.R. Sengelaub, Prenatal gonadal steroids affect adult spatial behavior, CA1 and CA3 pyramidal cell morphology in rats, Horm. Behav. 34 (1998) 183–198.
[27] J.J. Kim, M.S. Fanselow, Modality-specific retrograde amnesia of fear, Science 256 (1992) 675–677.
[28] M. Korte, O. Griesbeck, C. Gravel, P. Carroll, V. Staiger, H. Thoenen, T. Bonhoeffer, Virus-mediated gene transfer into hippocampal CA1 region restores long-term potentiation in brain-derived neurotrophic factor mutant mice, Proc. Natl. Acad. Sci. U. S. A. 93 (1996) 12547–21552.
[29] M.D. Madeira, M. Paula-Barbosa, A. Cadete-Leite, M.A. Tavares, Unbiased estimate of hippocampal granule cell numbers in hypothyroid and in sex–age-matched control rats, J. Hirnforsch. 29 (1988) 643–650.
[30] S. Maren, B. de Oca, M.S. Fanselow, Sex differences in hippocampal long-term potentiation (LTP) and Pavlovian fear conditioning in rats: positive correlation between LTP and contextual learning, Brain Res. 661 (1994) 25–34.
[31] A.L. Markowska, Sex dimorphisms in the rate of age-related decline in spatial memory: relevance to alterations in the estrous cycle, J. Neurosci. 19 (1999) 8122–8133.
[32] E.J. Markus, M. Zecevic, Sex differences and estrous cycle changes in hippocampus-dependent fear conditioning, Psychobiology 25 (1997) 246–252.
[33] B.S. McEwen, S.E. Alves, Estrogen actions in the central nervous system, Endocr. Rev. 20 (1999) 279–307.
[34] K.A. McNish, J.C. Gewirtz, M. Davis, Evidence of contextual fear after lesions of the hippocampus: a disruption of freezing but not fear-potentiated startle, J. Neurosci. 17 (1997) 9353–9360.
[35] M. Montminy, Transcriptional regulation by cyclic AMP, Annu. Rev. Biochem. 66 (1997) 807–822.
[36] T. Nabeshima, A. Katoh, H. Ishimaru, Y. Yoneda, K. Ogita, K. Murase, H. Ohtsuka, K. Inari, T. Fukuta, T. Kameyama, Carbon monoxide-induced delayed amnesia, delayed neuronal death and change in acetylcholine concentration in mice, J. Pharmacol. Exp. Ther. 256 (1991) 378–384.
[37] S.L. Patterson, L.M. Grove, P.A. Schwartzkroin, M. Bothwell, Neurotrophin expression in rat hippocampal slices: a stimulus paradigm inducing LTP in CA1 evokes increases in BDNF and NT-3 mRNAs, Neuron 9 (1992) 1081–1088.
[38] G. Paxinos, C. Watson, The Rat Rain, third edition, Academic Press, New York, 1997.
[39] R.G. Phillips, J.E. LeDoux, Differential contribution of amygdala and hippocampus to cued and contextual fear conditioning, Behav. Neurosci. 106 (1992) 274–285.
[40] R.G. Phillips, J.E. LeDoux, Lesions of the dorsal hippocampal formation interfere with background but not foreground contextual fear conditioning, Learn. Mem. 1 (1994) 34–44.
[41] M.M. Poo, Neurotrophins as synaptic modulators, Nat. Rev., Neurosci. 2 (2001) 24–32.
[42] C. Rampon, Y.-P. Tang, J. Goodhouse, E. Shimizu, M. Kyin, J.Z. Tsien, Enrichment induces structural changes and recovery from nonspatial memory deficits in CA1 NMDR1–knockout mice, Nat. Neurosci. 3 (2000) 238–244.
[43] R.L. Roof, M.D. Havens, Testosterone improves maze performance and induces development of a male hippocampus in females, Brain Res. 572 (1992) 310–313.
[44] G.E. Schafe, N.V. Nadel, G.M. Sullivan, A. Harris, J.E. LeDoux, Memory consolidation for contextual and auditory fear conditioning is dependent on protein synthesis, PKA, and MAP kinase, Learn. Mem. 6 (1999) 97–110.
[45] S. Schulz, H. Siemer, M. Krug, V. Höllt, Direct evidence for biphasic cAMP responsive element-binding protein phosphorylation during long-term potentiation in the rat dentate gyrus in vivo, J. Neurosci. 19 (1999) 5683–5692.
[46] M. Sheng, M.A. Thompson, M.E. Greenberg, CREB: a Ca^{2+}-regulated transcription factor phosphorylated by calmodulin-dependent kinases, Science 252 (1991) 1427–1430.
[47] A.J. Silva, R. Paylor, J.M. Wehner, S. Tonegawa, Impaired spatial learning in α-calcium–calmodulin kinase II mutant mice, Science 257 (1992) 206–211.
[48] L.R. Squire, Memory and the hippocampus: a synthesis from findings with rats, monkeys, and humans, Psychol. Rev. 99 (1992) 195–231.
[49] L. Stubley-Weatherly, J.W. Harding, J.W. Wright, Effects of discrete kainic acid-induced hippocampal lesions on spatial and contextual learning and memory in rats, Brain Res. 716 (1996) 29–38.
[50] S.M. Taubenfeld, K.A. Wiig, M.F. Bear, C.M. Alberini, A molecular correlate of memory and amnesia in the hippocampus, Nat. Neurosci. 2 (1999) 309–310.
[51] F. van Haaren, N.E. van de Poll, The effect of a choice alternative on sex differences in passive avoidance behavior, Physiol. Behav. 32 (1984) 211–215.
[52] F. van Haaren, A. van Hest, R.P.W. Heinsbroek, Behavioral differences between male and female rats: effects of gonadal hormones on learning and memory, Neurosci. Biobehav. Rev. 14 (1990) 23–33.
[53] G.E. Wood, T.J. Shors, Stress facilitates classical conditioning in males, but impairs classical conditioning in females through activational effects of ovarian hormones, Proc. Natl. Acad. Sci. U. S. A. 95 (1998) 4066–4071.
[54] J. Xing, D.D. Ginty, M.E. Greenberg, Coupling of the RAS-MAPK pathway to gene activation by RSK2, a growth factor-regulated CREB kinase, Science 273 (1996) 959–963.
[55] K.K. Yamamoto, G.A. Gonzalez, W.H. Biggs III, M.R. Montminy, Phosphorylation-induced binding and transcriptional efficacy of nuclear factor CREB, Nature 334 (1988) 494–498.
[56] J.C.P. Yin, J.S. Wallach, M. Del Vecchio, E.L. Wilder, H. Zhou, W.G. Quinn, T. Tully, Induction of a dominant negative CREB transgene specifically blocks long-term memory in *Drosophila*, Cell 79 (1994) 49–58.

THE JOURNAL OF COMPARATIVE NEUROLOGY 483:383–402 (2005)

Drebrin A Is a Postsynaptic Protein That Localizes In Vivo to the Submembranous Surface of Dendritic Sites Forming Excitatory Synapses

CHIYE AOKI,[1]* YUKO SEKINO,[2,3] KENJI HANAMURA,[2] SHO FUJISAWA,[1] VEERAVAN MAHADOMRONGKUL,[1] YONG REN,[2] AND TOMOAKI SHIRAO[2]*
[1]Center for Neural Science, New York University, New York, New York 10003
[2]Department of Neurobiology and Behavior, Gunma University Graduate School of Medicine, Maebashi, Gunma 371-8511, Japan
[3]Core Research for Evolution Science and Technology, Japan Science and Technology Corporation, Kawaguchi 332-0012, Japan

ABSTRACT

Drebrin A is a neuron-specific, actin binding protein. Evidence to date is from in vitro studies, consistently supporting the involvement of drebrin A in spinogenesis and synaptogenesis. We sought to determine whether drebrin A arrives at the plasma membrane of neurons, in vivo, in time to orchestrate spinogenesis and synaptogenesis. To this end, a new antibody was used to locate drebrin A in relation to electron microscopically imaged synapses during early postnatal days. Western blotting showed that drebrin A emerges at postnatal day (PNd) 6 and becomes progressively more associated with F-actin in the pellet fraction. Light microscopy showed high concentrations of drebrin A in the synaptic layers of the hippocampus and cortex. Electron microscopy revealed that drebrin A in these regions is located exclusively in dendrites both neonatally and in adulthood. In adulthood, nearly all of the synaptic drebrin A is within spines forming asymmetric excitatory synapses, verified by γ-aminobutyric acid (GABA) negativity. At PNd7, patches of drebrin A immunoreactivity were discretely localized to the submembranous surfaces of dendrites forming slight protrusions—protospines. The drebrin A sites exhibited only thin postsynaptic densities and lacked axonal associations or were contacted by axons that contained only a few vesicles. Yet, because of their immunoreactivity to the NR2B subunit of *N*-methyl-D-aspartate receptors and immunonegativity of axon terminals to GABA, these could be presumed to be nascent, excitatory synapses. Thus, drebrin A may be involved in organizing the dendritic pool of actin for the formation of spines and of axospinous excitatory synapses during early postnatal periods. J. Comp. Neurol. 483:383–402, 2005. © 2005 Wiley-Liss, Inc.

Indexing terms: synaptogenesis; F-actin; NR2B; NMDA receptor; cortex; hippocampus; electron microscopy; spinogenesis; proto-spines

Drebrins are F-actin binding proteins, first identified by their surging expression during synaptogenesis (Shirao et al., 1988; Shirao, 1995). Two isoforms of drebrin occur in mammals—drebrin E (embryonic form) and drebrin A (adult form; Shirao and Obata, 1986; Shirao et al., 1989; Hayashi et al., 1998), generated by alternative mRNA splicing from a single gene (Kojima et al., 1993). Both are expressed in neurons, but only drebrin A is neuron-specific (Shirao and Obata, 1986). Their cellular distributions have been studied using a monoclonal antibody, M2F6, that recognizes both the adult and embryonic isoforms. Within non-neuronal cells, drebrin E colocalizes with actin stress fibers along sites adhering to the substratum (Asada et al., 1994; Peitsch et al., 1999), while in cultured neurons, drebrins E and A localize to spines (Shirao et al., 1987; Hayashi et al., 1996), together with F-actin (Takahashi et al., 2003). Transfection of non-neuronal cells with drebrin A-cDNA leads to enhanced adhesion of these cells to the substratum (Ikeda et al.,

Grant sponsor: Ministry of Education, Science, Sports, and Culture of Japan; Grant number: Grants-in-Aid 12053209; Grant number: Japan Foundation for Aging and Health; Grant sponsor: National Institutes of Health; Grant number: R01-NS41091; Grant number: R01-EY13145; Grant number: P30 EY13079.

Drs. Aoki and Sekino contributed equally to this work.

*Correspondence to: Chiye Aoki, Center for Neural Science, New York University, 4 Washington Place, New York, NY 10003. E-mail: chiye@cns.nyu.edu or Tomoaki Shirao, Dept. of Neurobiology and Behavior, Gunma University Graduate School of Medicine, 3-39-22, Showamachi, Maebashi, 3718511. E-mail: tshirao@med.gunma-u.ac.jp

Received 5 July 2004; Revised 24 September 2004; Accepted 27 September 2004

DOI 10.1002/cne.20449

Published online in Wiley InterScience (www.interscience.wiley.com).

© 2005 WILEY-LISS, INC.

1995) and the appearance of neurite-like processes (Shirao et al., 1992), while transfection of cultured hippocampal neurons with drebrin A-cDNA causes dendritic spines to elongate (Hayashi and Shirao, 1999). These observations indicate that drebrin A may be involved in neurite extension and spine formation. Within cultured neurons, the arrival of drebrin A in spines precedes the arrival of PSD-95, and suppression of drebrin A using antisense oligonucleotide prevents the formation of PSD-95 clusters within spines (Takahashi et al., 2003). These more recent observations indicate that the molecular maturation of protospines into mature spines may be governed by the formation of drebrin A–actin complexes.

The two drebrin isoforms can be distinguished by using Western blots. Within the cortex and the hippocampus, drebrin E is the major isoform expressed in rat brains at postnatal day 7 (PNd7) and the slightly larger drebrin A isoform becomes more prevalent by PNd21 (Hayashi et al., 1998). These observations suggest a rapid conversion of drebrin isoforms during the phase of spine and synapse formation. Might the embryonic isoform, drebrin E, be involved in the initial formation of protospines or filopodia, with the adult isoform, drebrin A, taking over the subsequent steps to govern the molecular maturation of protospines? If so, one would predict that drebrin A appears only after the establishment of morphologically identifiable spine heads and that drebrin A remains in spines after synapses have become established.

In this study, the emergence of drebrin A within intact cortex and hippocampus was examined by using a newly generated antibody, DAS2. Unlike its predecessor, M2F6, DAS2 recognizes drebrin A selectively and does not recognize drebrin E. Also, unlike DAS1, the previously made anti-drebrin A antibody (Shirao et al., 1994), DAS2 is compatible with immunocytochemistry. Using DAS2, electron microscopy was used to analyze the distribution of drebrin A in relation to newly forming synapses. Within the cortex and hippocampus of postnatal day (PNd) 7 rats, newly forming presumptive synapses could be distinguished from well-established excitatory synapses, based on the scarcity of vesicles within the abutting axons, absence of postsynaptic densities (PSDs), and/or absence of spine necks. Adult tissue was also sampled for determining whether drebrin A occurs exclusively at asymmetric excitatory synapses or across a mixture of excitatory, inhibitory, and neuromodulatory synapses.

MATERIALS AND METHODS

Animals

For the light and electron microscopic studies, Wistar rats were purchased from Charles River and bred in the NYU animal center in accordance with the guidelines published in the NIH Guide for the Care and Use of Laboratory Animals. For the biochemical analyses, male Wistar rats at PNd 0, 2, 4, 6, 8, 10, 12, 14, 16, 18, and 20, and at 15-weeks postnatal were used. These Wistar rats were housed in the animal center of Gunma University Graduate School of Medicine.

All experiments were carried out according to the Animal Care and Experimentation Committee of Gunma University, Showa Campus and of New York University.

Subcellular fractionation

Animals were deeply anesthetized with ether inhalation and the specified brain regions were removed. Each tissue was homogenized by sonication in 10 volumes of 5 mM Tris-HCl, pH 7.5, 150 mM NaCl, 0.5 mM dithiothreitol, 1% NP-40, and protease inhibitors (1 μM leupeptin, 250 μM phenylmethyl sulfonyl fluoride, 2 μM pepstatin), yielding the crude fraction. The crude fraction was then centrifuged at 200,000 × g for 60 minutes at 4°C (Optima TLX Ultracentrifuge, Beckman Instrument, Fullerton, CA), so as to bring down the F-actin in the pellet fraction but to retain actin monomers (G-actin) in the supernatant (Fox, 1985; Crosbie et al., 1991). The supernatant thus obtained was considered a mixture of the cytosolic fraction plus some portion of the membranous proteins solubilized by NP-40. The pellet was washed once and suspended directly with the sodium dodecyl sulfate (SDS) sample buffer in preparation for Western blotting. For extraction experiments, the pellet was again homogenized by sonication in 10 volumes of the high salt buffer containing 1 M NaCl and was then centrifuged at 200,000 × g for 60 minutes at 4°C.

Use of the three anti-drebrin antibodies in Western blots to characterize the developmental changes in the expression of drebrin isoforms across brain regions

For the detection of specific isoforms of drebrin, the Western blot membranes were probed with the M2F6 monoclonal antibody (Medical and Biological Laboratories, Japan), previously shown to recognize both the E and the larger A isoforms (Shirao et al., 1994). Alternatively, the expression level of drebrin A was probed using the polyclonal antibody DAS1, which recognizes the amino acid sequences unique to the A isoform: 319–335, 342–353, and 354–363 (Shirao et al., 1994).

Because DAS1 was shown not to be compatible with immunocytochemistry, a new polyclonal antibody, DAS2, was generated for the present study. DAS2 was directed against peptide Phe-Ile-Lys-Ala Ser-Asp-Ser-Gly-Pro-Ser-Ser-Ser (residues 325–336) that is also unique to the adult form of drebrin (Shirao et al., 1992). DAS2 was purified by epitope selection, using the above polypeptide.

Proteins from equal wet weights of tissue were separated by polyacrylamide SDS gel electrophoresis and transferred to an Immobilon-P membrane (Millipore, Bedford, MA). Detection of immunoreactive bands was made using the ECL Western Blotting analysis system (Amersham, Buckinghamshire, UK). Further details of the methods appear elsewhere (Hayashi et al., 1998).

For quantitative analysis, signals were densitometrically quantified by the NIH-Image analysis system. Data were statistically analyzed by the Student's t test. All of the data were presented as a mean ± SEM.

Preparation of tissue for light and electron microscopy

Nine adult and 10 PNd7 Wistar rats were transcardially perfused with a mixture of aldehydes for fixation. All fixatives contained 0.1 M phosphate buffer (PB, pH 7.4) and 4% paraformaldehyde. For three of the adults and four of the neonates, 1% glutaraldehyde was added to the fixative. For two of the adults and three of the neonates, 3% acrolein was added to the fixatives. Slabs of brains

were sectioned in the sagittal or coronal plane, using a Vibratome, and fixation was terminated by reacting free-floating sections with 1% sodium borohydride made in 0.1 M PB. Sections were stored at 5°C, free-floating in a solution consisting of 0.9% sodium chloride (saline), 0.01 M phosphate buffer (pH 7.4), and 0.05% sodium azide (PBS–azide) to prevent bacterial growth.

Immunocytochemistry

The silver-intensified gold (SIG) was chosen as the label to optimize subcellular localization of drebrin A, while the horseradish peroxidase–diaminobenzidine (HRP-DAB) reaction product was used to maximize detection of drebrin A (Aoki et al., 2000). For both labeling procedures, sections were first treated to terminate the aldehyde fixation by immersing in a solution consisting of 1% hydrogen peroxide mixed in 0.1 M PB at room temperature for 30 minutes. These sections were incubated in a solution consisting of 0.01 M PB, saline (0.9% NaCl), and containing 1% bovine serum albumin (BSA) to minimize background immunolabeling and 0.05% sodium azide to minimize bacterial growth in the buffer. After preincubating sections for a minimum of 30 minutes, free-floating sections were incubated in the primary antibody solution, consisting of a 1:1,000 dilution of DAS2 in PBS–BSA–azide. The incubation was for 1 to 4 days at room temperature, under constant, gentle agitation. For immunolabeling that used the HRP reaction product as the label, the standard ABC Elite kit from Vector was used. For sections immunolabeled using SIG as the label, sections were incubated in a solution containing a 1:100 dilution of colloidal gold (0.8 nm) -conjugated goat anti-rabbit IgG, produced by Aurion (EM Sciences). The electron microscopy-grade silver-intensification kit (IntenSEM, Amersham) was used to enlarge the gold particles to sizes detectable by electron microscopy. Further details were as described previously (Aoki et al., 2000).

To determine whether the drebrin A-immunoreactive sites are contacted by glutamatergic or γ-aminobutyric acid (GABA)ergic terminals, two ultrastructural immunocytochemical tests were performed. One was to probe for the coexistence of drebrin A with the NR2B subunit of *N*-methyl-D-aspartate (NMDA) receptors along the postsynaptic membrane. The other was to probe for the presence of GABA within the axons positioned presynaptically to the drebrin A-site. The immunodetection of GABA and the NR2B subunits followed Phend's postembedding gold immunolabeling procedure (PEG; Phend et al., 1995) but with slight modifications, as described previously (Erisir et al., 2001; Fujisawa and Aoki, 2003). The NR2B subunit antibody was purchased from Upstate Technology (New York) and used at a dilution of 1:40. The rabbit anti-GABA antibody was purchased from Sigma and used at a dilution of 1:1,000.

Controls for immunocytochemistry

Specificity of the drebrin A antibody, DAS1, has been published previously (Shirao et al., 1994). Selectivity of the new anti-drebrin A antibody, DAS2, to drebrin A was determined by verifying that the antibody recognized a single band in Western blots (Fig. 1, right) corresponding to the upper of the two bands recognized by the monoclonal antibody, M2F6. In a previous study, the two bands recognized by M2F6 were shown to be drebrin E (lower band) and drebrin A (upper band; Shirao et al., 1994).

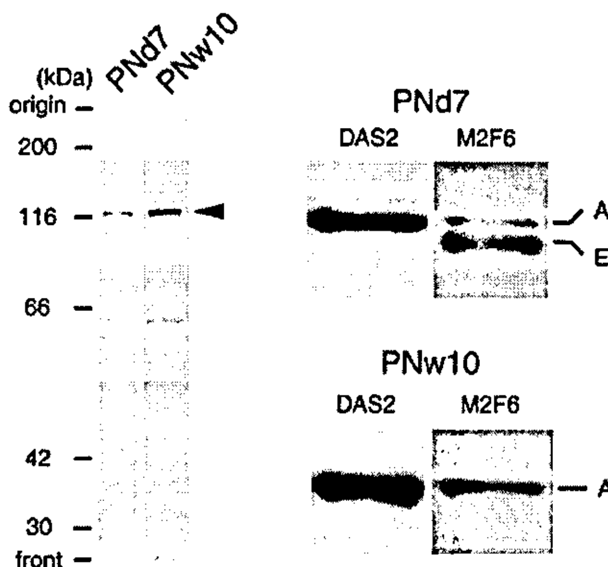

Fig. 1. Specificity of the new drebrin A antibody, DAS2 as revealed by Western blotting. The protein extract equivalent to 0.20 mg of wet weight tissue was analyzed by Western blotting. Left column: Western blot analysis using 8% gel showed that DAS2 antibody recognized a single band (arrowhead), both in postnatal day 7 (PNd7) and postnatal week 10 (PNw10) rat hippocampi. Right column: Top panel is a Western blot of PNd7 rat hippocampus using 5% gel. The monoclonal antibody M2F6 detected a faint band of drebrin A (A, upper band) in addition of major band of drebrin E (E, lower band), as reported earlier (Shirao et al., 1989; Imamura et al., 1992). DAS2 antibody recognized drebrin A but not drebrin E. Bottom panel: Western blot of PNw10 hippocampus. Both of M2F6 and DAS2 antibodies detected a single band.

Within homogenates prepared from hippocampi of PNd7 and postnatal week 10 (PNw10), the new DAS2 antibody did not recognize any protein band other than drebrin A (left column of Fig. 1).

Further controls for immunocytochemistry were performed using sections that were semiadjacent to the ones used for immunocytochemistry. The control sections were treated exactly as described under the Immunocytochemistry section above, except that the primary antibody was omitted. This resulted in complete elimination of immunoreactivity for drebrin A, GABA, and the NR2B subunit of NMDA receptors. In addition, preadsorption control for the DAS2 antibody was performed. As noted above, DAS2 was purified by epitope selection, using the synthetic polypeptide corresponding to the amino acid sequence unique to drebrin A. The same synthetic peptide was added to the DAS2 antibody solution at a concentration of 1 mg/ml at 37°C for 1 hour to preadsorb the primary antibody. The preadsorption caused great reduction of immunoreactivity within semiadjacent sections (further details described under the Results section).

Specificity of GABA labeling was further verified electron microscopically, based on the abundance of PEG within axon terminals forming axosomatic symmetric synapses and the relative scarcity of PEG with axon terminals forming asymmetric axospinous synapses (less than 1/30th of the colloidal gold/terminal content observed at symmetric synapses). This outcome was similar to the

results shown previously from this laboratory (Erisir et al., 2001) and by others (Megias et al., 2001).

Viewing of immunocytochemically stained sections

Sections were mounted on slides, coverslipped, and viewed using the light microscope. For electron microscopy, sections were further fixed using 1% osmium tetroxide, embedded in Embed 812, ultrathin-sectioned, and viewed under the JEOL 1200XL electron microscope. HRP-labeled sections were viewed without counterstaining, so as to optimize detection of low levels of reaction products along the membrane. SIG-labeled sections were counterstained with Reynold's lead citrate, because SIG labels could still be identified against the contrast-enhanced images of the neuropil. Images were captured both on film and digitally by using the Hamamatsu CCD camera from AMT (Boston, MA).

Ultrastructural analysis

Samples from the neocortex and hippocampus of five adult brains and four neonatal brains were collected for ultrastructural analyses, using an electron microscope. Digitally captured images were used to quantify the areal density of synaptic junctions and of immunolabeled processes, using the Hamamatsu CCD camera and the data acquisition system of AMT.

Processes were identified as axon terminals, based on the presence of vesicles and absence of microtubules. Conversely, dendritic shafts were identified by the absence of vesicles and, most often, also by the presence of microtubules. The putatively postsynaptic sites within neonatal tissue were identified by their juxtaposition to processes that were more clearly identifiable as axonal processes.

Where possible, junctions were identified as symmetric vs. asymmetric, based on the absence vs. presence, respectively, of PSDs. Junctions were also identified as forming on a dendritic shaft vs. a spine. The spines were distinguished from shafts, based on the absence of mitochondria or of microtubules or of vesicles in the cytoplasm.

The morphological criteria used to judge a synapse as mature and asymmetric were as follows: Parallel alignment of the dendritic and axonal plasma membranes; a collection of vesicles that are closely bounded by the plasma membrane or clustered near the presynaptic plasma membrane; presence of the PSD; and narrowing of the neck, if the synapse was on a spine. All of the axospinous junctions within adult tissue exhibited all of these characteristics, whereas few within PNd7 tissue exhibited all of these characteristics. This finding indicated that our criteria were useful for discriminating immature from mature synapses. Most of the asymmetric synapses of PNd7 tissue showed one or more of the following features: spine heads in which the neck was not narrowed; PSDs that are detectable but thin; and presynaptic profiles with only a few vesicles, most of which were at sites removed from the junction. Intercellular junctions exhibiting any of these features were categorized as presumptive immature synapses.

In neonatal tissue only, processes sometimes came in direct contact and were immunolabeled at contact sites but neither side could be identified as axonal or dendritic. These were categorized as junctional but were excluded from the "presumptive immature synapse" category. Protrusions along the plasma membrane of dendrites for which the axonal partner could not be identified were referred to as nonjunctional protospines and also excluded from the presumptive immature synapse category.

Within adult tissue, synapses on dendritic shafts and somata sometimes lacked PSDs. These were categorized as symmetric synapses. Within PNd7 tissue, only those synapses exhibiting more than four vesicles near the cleft, yet lacking PSDs, were categorized as symmetric and mature.

The synapse categories described above are congruent with previously accepted categories for symmetric (inhibitory) and asymmetric (excitatory) synapses within adult and developing tissue (Purpura and Pappas, 1972; Vaughn, 1989; Harris, 1999; Megias et al., 2001; Marty et al., 2002; Peters, 2002; Minelli et al., 2003).

Quantitative analysis of synapses

Quantitative analysis of HRP-labeled adult tissue was performed upon immunolabeled synaptic profiles collected from 36 nonoverlapping fields, with each field encompassing 12.25 μm^2. We determined the proportion among the encountered synapses that were or were not labeled, labeled pre- or postsynaptically, at an asymmetric or a symmetric synapse, and formed on a dendritic spine or a dendritic shaft. Quantitative analysis of HRP-labeled PNd7 tissue was performed similarly, by categorizing the randomly encountered synapses from 26 nonoverlapping fields into groups that were or were not labeled, labeled pre- or postsynaptically, at a symmetric or an asymmetric synapses, and with immature or mature morphological features.

Further quantitative analysis was performed for the cortex. Comparisons across the two ages (PNd7 vs. adult) was made by dividing the encountered synapses randomly into 10 groups for the PNd7 tissue and into 13 groups for the adult tissue, calculating the percentage of synapses encountered (mature or immature) for each group that were immunolabeled or not immunolabeled. Unpaired t test (two-tailed) was performed to determine whether the mean percentage value of unlabeled synapses was different across the two ages.

Quantitative analysis of the proximity of drebrin A immunoreactivity to the plasma membrane

The nondiffusible immunolabel, SIG, was used to analyze the proximity of drebrin A immunoreactivity to the plasma membrane. SIG-labeled tissue were sampled from two PNd7 and two adult brains. The proximity of SIG particles to the plasma membrane was assessed by measuring the distance, in nanometers, from the center of the silver grains to the inner surface of plasma membranes. The proximity of SIG particles to the plasma membrane, relative to the diameter of the immunolabeled profiles, was also assessed. Histograms were prepared, based on 250 SIG particles collected from 39 nonoverlapping fields of adult tissue and 80 SIG particles collected from 14 nonoverlapping PNd7 tissues.

Photomicrograph presentation

Images were captured digitally by using AMT System's CCD camera or directly on electron microscopy negatives. The captured images were cropped, contrast-enhanced when needed, and labeled to identify structures using the Adobe Photoshop software (version 6.0).